Insights into artificial water oxidation—A computational perspective

Schilling, Mauro ; Luber, Sandra

Abstract: Numerous researchers around the globe are focusing their efforts toward the development of renewable energy sources. Among them are devices that harvest sun light and use it to split water into molecular hydrogen and oxygen. Thereby water oxidation is believed to be one of the bottlenecks that needs to be overcome through the development of appropriate catalysts. An in-depth understanding of the fundamental properties of those catalysts is crucial in order to improve them further or to design novel catalysts with high catalytic activity and stability. Theoretical studies offer a great opportunity, to elucidate the structure and dynamics of the catalyst, the catalytic mechanism, and the properties of potential intermediates. In this chapter, we describe our recent efforts for advanced modeling of catalysis and how the combined effort of experimental and computational work can lead to a better understanding of the catalysts at hand and development of new catalysts. Thereby we focus on two families of catalysts studied by our group. First we introduce tetranuclear Co(II)-based water oxidation catalysts featuring a cubane core as found in the oxygen evolving complex of nature's photosystem II. Afterward, we discuss selected mononuclear Ru(II)-based water oxidation catalysts.

DOI: https://doi.org/10.1016/bs.adioch.2019.03.001

Originally published at:
Schilling, Mauro; Luber, Sandra (2019). Insights into artificial water oxidation—A computational perspective. In: Van Eldik, Rudi; Hubbard, C D. Advances in Inorganic Chemistry. San Diego: Elsevier, 61-114.
DOI: https://doi.org/10.1016/bs.adioch.2019.03.001

Theoretical insights into artificial Water Oxidation

Mauro Schilling, Sandra Luber*

University of Zurich

Winterthurerstrasse 190, Zurich

Abstract

Numerous researchers around the globe are focusing their efforts towards the development of renewable energy sources. Among them are devices that harvest sun light and use it to split water into molecular hydrogen and oxygen. Thereby water oxidation is believed to be one of the bottle-necks that needs to be overcome through the development of appropriate catalysts. An in depth understanding of the fundamental properties of those catalysts is crucial in order to improve them further or to design novel catalysts with high catalytic activity and stability. Theoretical studies offer a great opportunity, to elucidate the structure and dynamics of the catalyst, the catalytic mechanism and the properties of potential intermediates. In this chapter, we describe our recent efforts for advanced modeling of catalysis and how the combined effort of experimental and computational work can lead to a better understanding of the catalysts at hand and development of new catalysts. Thereby we focus on two families of catalysts studied by our group. First we introduce tetranuclear Co(II)-based water oxidation catalysts featuring a cubane core as found in the oxygen evolving complex of nature's photosystem II. Afterwards, we discuss selected mononuclear Ru(II)-based water oxidation catalysts.

Keywords: water oxidation, computational chemistry, *ab initio* molecular dynamics, cubanes, ruthenium catalysts, water nucleophilic attack, interaction of two metal oxo-species (I2M), solvation effects, rational ligand design, in silico design, density functional theory, reaction mechanism

1. Introduction

1.1. Artificial Water Splitting - a Short Overview

Almost on a daily basis, the news report extreme weather phenomena or new records in terms of temperature, rainfall, or winds. Some of the extreme conditions, such as droughts, are believed to be the direct or indirect consequences of man made climate change[1–3]. In 2015, most countries in the world agreed by signing the *Paris agreement*, which has the aim to limit the rise of the average global temperature to below 2°C above pre-industrial area, and to take actions against man made climate change, especially by reducing the emission of greenhouse gases as well as by the development of clean, renewable energy sources[4]. Among others, photovoltaic modules are used to harvest energy provided by the sun and convert it to an electric potential. However, the efficiency of the latter is strongly dependent on the latitude, the local climate (e.g. seasons), the elevation and of course the daytime. In particular, the daily peak in energy production around noon causes some problems, since the energy consumption of mankind normally peaks in the evening. This results in a mismatch in production and consumption, which is often referred to as 'Duck curve'[5]. In order to overcome this problem, development of energy storage and transport capabilities have seen a lot of scientific interest in the recent past.

Nature has already solved this problem billions of years ago with a process called photosynthesis. The latter describes a combination of photo- and electrochemical reactions performed by a complex array of enzymes that - in an ingenious assembly - take advantage of compartmentalization within cells. Chemically, photosynthesis might be divided into two parts - water oxidation and CO_2 reduction. The first part, water oxidation, is related to conversion of sun light energy into a chemical potential, which is 'stored' in the form of chemical bonds in the second part. An analogous process - water splitting - is artificially achieved by electrolysis where water is split into O_2 and H_2. The efficiency of this process relies heavily on the nature of the electrode, which is often composed of platinum. The availability of the latter limits economically

viable implementation of this process on a global scale. Further, in its classical implementation electrolysis is driven by an electric current rather than by sunlight. The use of electric energy produced from renewable sources is possible, however this is an indirect pathway which may contain many interfaces between different devices. Complex assemblies of multiple devices are in general prone to losses. Those losses may sum up to an overall efficiency which may not be economically sustainable yet. It would therefore be desirable to develop processes where sunlight is directly stored in chemical bonds - such processes are called 'artificial photosynthesis'. This term is somewhat ambiguous, since it does not specify in which form i.e. in what kind of chemical bonds the sunlight energy is stored, be it H_2, or as in nature in the form of C−H bonds.

In the field of heterogeneous catalysis there are already systems known which are up to the task. Some of them such as Nocera's wireless solar water splitting device are also known as 'artificial leafs'[6,7]. The main drawback of such complex assemblies is that a systematic improvement of specific properties like the catalytic efficiency or lifetime is often very difficult. Therefore groups of researchers often focus only on a single part of the whole process, be it light harvesting, water oxidation or water reduction, in the hope to master each piece individually and combining them in the end. However, the heterogeneous nature of the catalysts used to drive those processes often does not allow for a mechanistic insight on a molecular level, knowledge of which might be crucial in order to understand the advantages and disadvantages of the use of certain materials, and could in principle help to improve systematically existing catalysts or even serve to develop guidelines for the design of new ones.

Therefore homogeneous catalysts might be a suitable alternative. Their well defined molecular structure in principle allows for in-depth mechanistic studies that could lead to the identification of potential bottlenecks in the catalytic process. Of course homogeneous catalysts also come with a drawback - many of them suffer from stability issues under catalytic conditions, and addressing these is often difficult. As for the heterogeneous catalysts the final goal is their integration into a single device. Attempts in this direction have already

been made, among them is a functioning water-splitting device based on an immobilized, but not covalently linked Ru based water oxidation catalyst by Sun and co-workers[8]. However it is a mere proof of concept rather than an scalable device which may soon enter application on an industrial scale.

1.2. Water Oxidation Reaction

In the following we will focus our attention on the oxidative part of the water splitting process which is often recalled to be the bottleneck of the whole process. The overall chemical reaction for water oxidation is:

$$2\,H_2O \longrightarrow 4\,H^+ + O_2 + 4\,e^-. \tag{1}$$

The half-reaction itself is endothermic, which means that 113.5 kcal/mol (4.92 eV, at standard conditions) in terms of free energy are required in order to drive the reaction. This is the thermodynamic minimum, assuming no further kinetic barriers for chemical reactions such as the O−O bond formation, reactant association or product release, which can only be achieved in a hypothetical ideal system. In practice those barriers turned out to be significantly large, in particular due to the complexity of the reaction which consists of four consecutive oxidation and deprotonation reactions and an O−O bond formation. To match the thermodynamics of an ideal process is on a purely theoretical level the main goal in catalyst development. However a catalyst that has the potential to play a crucial role in upcoming energy supply chains based on renewable energy sources has to fulfill other requirements as well. The latter might be defined as[9,10]: (1) efficiency - high activity under mild conditions (neutral pH, room temperature, atmospheric pressure); (2) specificity - towards a single product which might be easy to separate from the reaction; (3) durability - longterm stability in order to achieve high turnover numbers or a facile recycling and regeneration process; (4) cleanliness - environmentally friendly i.e. 'green chemistry', non-toxic components; (5) adaptability - easy to modify e.g. for different conditions, to immobilize on surfaces, or to couple with different catalysts. Most of those criteria are interdependent and cannot be individually

targeted when developing novel catalysts. Therefore in a first step, one often primarily aims for efficiency. Here, theoretical studies can be crucial in order to understand the fundamental properties of the catalyst, in particular, when attempting to lower the activation barrier of the rate-determining step. The latter requires knowledge on intermediates that are part of the catalytic cycle. The elusive nature of the latter often makes theoretical modeling a premise in to order to come up with a conclusive mechanistic proposal.

In the past decade numerous molecular water oxidation catalysts (WOCs) have been proposed, most of them contain transition metals - primarily Mn, Fe, Co, Ru, and Ir. However there are also examples known that contain Ni or Cu[11–16]. For some of those catalysts there exist mechanistic proposals which are either based on experiments, theory or in the best case a combination of both[17–22].

While the detailed mechanisms are dependent on the nature of the catalyst, all of them share some common features. We recently reviewed the recent mechanistic studies on molecular cobalt based WOCs, where we highlighted the similarities of the different catalysts in terms of their proposed mechanisms[10]. In order to lay the foundation for the following sections, we will give a brief overview of the most general concepts in terms of water oxidation and modeling of the latter.

2. Water Oxidation - a Mechanistic Perspective

Catalytic water oxidation can be divided into the following stages: (1) water activation, i.e. oxidation and deprotonation in order to reach a metal-oxo (M=O) intermediate, (2) oxygen-oxygen bond formation, for which there are two general possibilities: a water nucleophilic attack (WNA) or an interaction of two metal-oxo (I2M), sometimes also referred to as radical coupling (RC); depending on the nature of the catalysts there are many variations of those two reactions (see Fig. 2). (3) release of O_2, determined by the O−O bond formation mechanism; either further oxidations are required or O_2 is directly released

from the catalyst. (4) regeneration of the catalyst by association of a water molecule. This step might happen in a concerted fashion with the previous step. A generalized catalytic cycle is shown in Figure 1.

[Figure 1 about here.]

The initial stage of the catalytic cycle is characterized by electron transfers (ETs) and proton transfer (PT) reactions or vice versa. In order to avoid the accumulation of charge, ET reactions are normally directly followed by PT reactions. If those two happen together in a concerted process then they are referred to as a proton coupled electron transfer (PCET). Several ETs and PTs or PCETs lead to a metal-oxo species, which is a prerequisite for the O−O bond formation. The origin of the high reactivity of those metal-oxo species is often uncertain as we will elucidate with the following example.

For the sake of simplicity, let us assume that a model catalyst is only composed of a single metal center, which in its resting state bears a single aqua ligand - $\{\mathrm{M{-}OH_2}\}^{n+}$. After two consecutive PCETs, the metal-oxo species $\{\mathrm{M{=}O}\}^{n+}$ is reached. The Lewis formula of the latter is somewhat misleading, depending on the electron counting method - ionic ($\mathrm{M}^{+(\mathrm{n+II})} + \mathrm{O}^{-\mathrm{II}}$) or neutral ($\mathrm{M}^{+n} + \mathrm{O}^{0}$) - a different formal oxidation state might be assigned to the metal center. Further, for the metal-oxo species there are resonance structures i.e. $\{\mathrm{M{=}O}\} \longleftrightarrow \{\mathrm{M{-}O\cdot}\}$, suggesting another possible formal oxidation state of $\mathrm{M}^{+(\mathrm{n+I})} + \mathrm{O}^{-\mathrm{I}}$. The oxyl formalism implies on one hand a weaker metal-ligand interaction, and on the other hand a higher reactivity of the ligand due to its radical character. The metal-ligand interaction is expected to increase for highly oxidized species i.e. n = 5 or higher, where most of the metal's 3d orbitals are empty. For those species one might draw the structure as $\{\mathrm{M{=}O}\} \longleftrightarrow \{\mathrm{M{\equiv}O}\}$, where the formal oxidation states are $\mathrm{M}^{+(\mathrm{n-I})} + \mathrm{O}^{+\mathrm{I}}$. Here, the +I oxidation state of the ligand highlights its electrophilic character, in the case of neutral counting[23].

We have to keep in mind that oxidation states are a mere bookkeeping tool for the number of electrons in the system. There is no rigorous quantum chemi-

cal definition of oxidation states and in particular in transition metal complexes assignment of formal oxidation states might lead to contradictory interpretations. However, theoretical chemistry offers several techniques to deduce formal oxidation states from the total electron density or wavefunction such as Bader, Voronoi, Mulliken, or Löwdin charges to mention the most popular ones (see Ref.[24] and references therein). More advanced concepts are based on the localization of the electron density onto various kinds of atom centered orbitals[24–28].

2.1. Theoretical Description of Metal-Oxo Species

By drawing Lewis structures one might oversimplify the description of the metal-oxo species too. While $\{\mathrm{M}-\mathrm{O}^{\bullet}\}^{(n)+}$ implies that there is an unpaired electron, it by no means gives any information on its localization with respect to the oxygen atom. The latter becomes obvious when it comes to the description of real catalysts such as a triplet Mn^{V}=O complex, that was studied by Ashley and Baik[23]. Based on their theoretical calculations, they assigned the two unpaired electrons that define the triplet state to the non-bonding molecular orbital with d_{xy} symmetry and π^*_{M-Oxo} molecular orbital, visualizing of which is beyond the capabilities of Lewis structures.

Therefore the possibility to draw several different resonance structures asks for a solid quantum chemical description in order to pin-down the 'true' nature of the species. Nowadays, the workhorse of quantum chemistry is Kohn-Sham density functional theory (KS-DFT). As a single determinant method DFT usually struggles to describe correctly structures like the oxo/oxyl if the real structure is a mixture of these two structures. In order to describe this ambivalence multi-configurational self-consistent field (MCSCF) approaches such as complete active space self-consistent-field (CASSCF)[29], restricted active space self-consistent-field (RASSCF)[30,31], and generalized active space self-consistent-field (GASSCF)[30,32,33] calculations can be used. Those methods are non-trivial in their application and are due to their high computational cost only applicable for smaller systems or for very specific questions. It is therefore common to use MCSCF calculations as a benchmark for DFT calculations employing different

exchange-correlation functionals. A common observation thereby is that the use of hybrid functionals is required, and that especially the amount of Hartree-Fock (HF) exchange plays a crucial role when it comes to describe metal-oxo species[23,34]. This is also true for activation energies for the O−O bond formation. Ashley and Baik reported for both the WNA- and the RC-mechanism of a Mn-based WOC a non-trivial relation between the % of HF-exchange and the barrier height. In case of a WNA, they found the activation energy to be a function of the amount of HF-exchange, i.e. larger HF contributions led to a higher activation energy. At the same time, the energetic difference between barriers obtained for high-spin state (in their case triplet) and low-spin state (here singlet) diminished and both spin-states converged to the same barrier. For the RC mechanism, the energetic difference between barriers obtained for HS and LS configurations also decreased but it did not vanish within the probed range[23]. Inspecting the oxyl character of those species revealed that the barrier of neither the WNA nor the RC mechanism was directly dependent on the oxyl character i.e. there was no obvious benefit of a large amount of radical character.

Together with the ever growing computational resources and recent developments such as the domain-based local pair natural orbital framework, even wavefunction based methods such as CCSD(T) become feasible for transition metals, which might in the future be a viable alternative to MCSCF methods[35–37].

2.2. Mechanistic Proposals for the Oxygen-Oxygen Bond Formation

We already briefly introduced the WNA and RC mechanism. In this paragraph we focus on the different variations of those mechanisms (see Fig. 2)[38]. While in principle there are several reaction pathways imaginable for each catalyst, usually only a few of them are plausible under the applied reaction conditions. Ideally water oxidation takes place at a neutral pH, however depending on the catalyst and / or the use of photosensitizer or sacrificial oxidants, different conditions might be used. For example, the performance of most Ru-based

WOCs is evaluated in the presence of the chemical oxidant cerium-ammonium-nitrate (CAN) under acidic conditions (pH = 1). In the case of an intermolecular WNA, a water molecule from the solvent has to attack nucleophilically the metal-oxo species, forming a formal $\{M-OOH_2\}$ species, which presumably quickly deprotonates to form the corresponding $\{M-OOH\}$ species. However, it is probably more realistic to assume that the oxygen-oxygen bond formation and the deprotonation take place in a concerted manner. Further, the weak nucleophilicity of the water molecules might be enhanced by the presence of a base, be it intra or intermolecular. Thereby the base does not necessarily have to interact with the nucleophile itself. An indirect participation in a proton reshuffling process during the O−O bond formation might also be possible, as has been suggested for several catalysts[39–42].

When the intramolecular base is not an integral part of the ligand framework, but rather a species such as a hydroxide coordinated to a second metal center, as might be the case in heterogeneous or polynuclear catalysts, then more options for the O−O bond formation arise. First, the hydroxido ligand might act as a nucleophile in an intramolecular WNA. Secondly upon further oxidation a second metal-oxo might be formed which could undergo the O−O bond formation in an intramolecular RC fashion. An RC mechanism is also possible if the O−O reaction is bimolecular, i.e. when two $\{M=O\}$ species dimerize to form the O−O bond. The ability of catalysts to dimerize is strongly dependent on their respective ligand spheres, that should be able to stabilize a face-to-face orientation of the $\{M=O\}$ intermediates.

Experimentally it is difficult to distinguish between the different reaction pathways discussed above. Often the only easily accessible information is the reaction-order derived from the rate equation. However, the latter only allows to differentiate a second-order reaction such as a O−O bond formation in an intermolecular RC from all the other possibilities shown in Figure 2 as all of them are first-order in terms of the catalyst concentration. Another common experiment is the use of isotopically labeled water during the synthesis of the catalyst or as a solvent during water oxidation, in order to identify the source

of the released O_2 [43]. However, the extent to which such studies can help to identify the O−O mechanism strongly depends on the system at hand.

[Figure 2 about here.]

2.3. Energetics of the Oxygen-Oxygen Bond Formation

Theoretical studies can provide much-needed insight by comparing different routes in terms of their energetics. Besided the thermodynamics, the kinetics of chemical steps are also of interest, knowledge of which can be gained from transition states connecting possible intermediates of the catalytic cycle. Calculating transition states is a non-trivial task and often requires chemical intuition. Nevertheless, there are several standard protocols available. In the following we will shortly introduce the basic principles of some selected methods.

Transition states are saddle points on the potential energy surface. The most common approach to converge a structure to such a point is to calculate the second derivatives (Hessian matrix), identify an eigenvector with a negative eigenvalue which corresponds to the reaction coordinate and maximize the energy with respect to this eigenvector, while minimizing it in all other directions. This method usually requires a good initial guess that is already close to the transition state. If only the reactant and product of a reaction are known, then methods like self-consistent reaction path optimization [44] or nudged-elastic-band (NEB) methods might be applied [45,46]. In order to find the minimum energy pathway (MEP) connecting two minima, i.e. the reactant and the product, several intermediate structures (also referred to as beads) along this pathway have to be optimized. In the case of NEB calculations, those beads are connected by springs which ensure an equal spacing along the pathway. The energy of those beads is minimized with respect to all degrees of freedom perpendicular to the springs. When the climbing-image (CI) extension to the NEB methodology is used, where the bead with the highest energy is allowed to move along the band, then the converged MEP is guaranteed to contain the saddle point.

Both methods discussed so far rely on the fact that the reaction coordinate is rather simple and might even be guessed by experienced chemists. This dis-

advantage might be overcome or at least reduced by using sampling techniques based on molecular dynamics or Monte Carlo. In the limit of infinite sampling time, such sampling techniques would allow to reconstruct the whole potential energy surface. However, in order to limit the computational effort enhanced sampling techniques might be applied that force the systems to explore areas of interest. There are numerous techniques for this purpose, and we will shortly introduce only one of them - metadynamics[47,48]. This technique is based on the continuous addition of an artificial bias potential during a molecular dynamics simulation in order to discourage revisiting the same state again.

States are defined in terms of collective variables i.e. components of the reaction coordinate that are able to distinguish unambiguously between the reactant and product. *A priori* there is no previous knowledge on the reaction path or transition state required, however metadynamics simulations depend on many parameters, such as the height and width of the gaussians that are continuously added to the bias potential, the frequency in which those gaussians are spawned and of course the collective variables which define the area of the potential energy surface to be explored. Even properly set parameters sometimes do not lead to convergence of the free energy within a reasonable time frame, therefore there are many extensions such as well-tempered and transition-tempered metadynamics that might help to facilitate this process in certain cases[49–51].

2.4. How to Account for the Surrounding Solvent?

Even though sampling techniques such as metadynamics come with extraordinary high computational costs, they are often the method of choice if solvation effects are to be treated explicitly in a dynamic manner. This is true in particular for the O−O bond formation by a WNA where the nucleophile stems from the solvation shell. So far, the immense computational cost and the non trivial application of those methods, in particular in the case when both the catalyst and the solvent are described by DFT, have effectively limited their application to complex systems in the field of homogeneous transition metal-based catalysis. Nevertheless there are a few examples[42,52–54].

Originally, sampling techniques such as molecular dynamics were developed in the context of an entirely classical description based on molecular mechanics (MM). However, transition metal complexes that participate in e.g. bond-formation and -breaking reactions, which may go along with a change of the local electronic structure at the metal center, are difficult to describe in a classical sense by means of a force field. Nonetheless, recently the first classical simulations of a solvated Ru-based WOC appeared[55,56], where the empiric valence bond approach[57] was used to obtain a detailed picture of the O−O bond formation by an intermolecular RC mechanism.

In order to represent the electronic structure of transition metal complexes sufficiently accurate DFT or post-HF methods are usually required. Both worlds, i.e. quantum mechanics (QM) and MM might be combined in the so called QM/MM methodology, where different parts of the system are calculated at a different level of theory. For example, in the case of solvated transition metal complexes, the solute i.e. the catalyst, can be described employing DFT while the solvent molecules can be treated classically. The latter works in particular well when the studied reactions such as the O−O bond formation are intramolecular, i.e. there is no bonding interaction between the solute and solvent. In this case the QM/MM methodology used in a dynamic setup offers additional insight at significantly reduced cost compared to a full *ab initio* molecular dynamics (AIMD) setup[58].

In general one differentiates between implicit and explicit solvation. Implicit solvation aims to capture the average effects of solute-solvent interactions but has shortcomings when it comes to describe directed interactions such as hydrogen bonding. While there are different formulations of such solvation models, such as the well known polarizable continuum model (PCM) and conductor like screening model (COSMO)[59], their basic principle is similar. The solvent is approximated as an electrostatic potential interacting with the potential created by the solute. The models differ in the formulation of those interactions as well as the description of the interface region between the charged cavity surrounding the solute and the solvent continuum[60–63]. Further, those solvation models

rely on an empirical parametrization to reproduce experimental solvation free energies. The parametrization is often based on a limited set of small to medium sized (neutral) organic molecules and is done at a rather low level of theory, e.g. small basis set[64,65]. Thus the application of implicit solvation models to more complex systems such as transition metal complexes might not in all cases be justified[66].

While implicit solvation models are known to perform reasonably well for systems with no direct solute-solvent interaction, they often struggle when such interactions become important. This is for example the case for the O–O bond formation by a WNA mechanism. Unless there is a basic site in close proximity to the newly formed O–O bond, a high energy $\{M-OOH_2\}$ species would be formed. It has therefore become customary to incorporate several water molecules into the model systems, that might act as proton acceptor or proton shuttles[39–42,67]. The atomistic description of the solute-solvent interactions is referred to as explicit solvation, and might also be combined with implicit solvation to account for the interaction with the bulk solvent. Such a static approach using geometry optimizations is normally limited to a small number of explicit solvent molecules, because solvent molecules do not only interact with the solute but also with other solvent molecules. The various possible solvent configurations can lead to a strongly corrugated energy surface, where comparing energies of different solutes, as there are in a catalytic cycle. We explored the limits of this approach in some of our studies which are discussed later on in detail (see Section 3)[54]. With COSMO for realistic solvents (COSMO-RS) an attempt was made to overcome the limitations of a 'simple' implicit solvation model. The method is based on quantifying intermolecular electrostatic and hydrogen-bond interactions using the COSMO polarization charge densities, resulting in a more realistic description of the solvent[59].

2.5. Reduction Potentials and pK_a Values

The choice of the solvation model does not only affect the computational results of catalytic mechanisms, related structures and energies, but also other

key properties such as reduction potentials and pK_a values. Even though the access to the latter is experimentally often restricted to a limited set of species, theoretical estimates are still of great importance when it comes to judging which species might be present in solution during catalysis.

Depending on the solvation model there are several protocols available to calculate reduction potentials and pK_a values[68,69]. When employing an implicit solvation model, usually thermodynamic cycles, also known as Born-Haber cycles, are normally used. Those cycles avoid the calculation of a formal H^+ or e^- in solution, by calculating their respective solvation free energies instead[70]. In case the reaction is formulated in an isodesmic manner, either a proton or an electron is transfered to a corresponding base or oxidant instead of being released into the solution. The latter might lead to more favorable error cancellation, if all the participants of the reaction are similar in their composition, and if they are calculated at the same level of theory[71]. If solvent-solute interactions play a significant role in determining the structure of the reactants and/or the products, then thermodynamic cycles - that rely on the assumption that the chemical structure of a species remains the same upon solution - are not applicable anymore[72]. For certain systems such as transition-metal ions, it turned out that not only the molecules in the first coordination sphere but also those in the second shell have to be described explicitly in order to reproduce experimental reduction potentials[73]. As already discussed, the inclusion of explicit solvent molecules in principle makes the use of sampling techniques necessary. An alternative might be COSMO-RS, which has been shown to be able to reproduce experimental reduction potentials with a better accuracy than other common implicit solvation models, even without inclusion of molecules in the second coordination sphere[74]. A drawback of the methodology discussed above is its evident failure for highly charged species, for which solvent continuum models are usually not parameterized. The latter can be overcome if the charged complexes are neutralized for example by the addition or the removal of protons. The reduction potential of the highly charged species, can then be obtained by calculating several thermodynamic cycles consisting of inter-

mediate species that carry a smaller molecular charge. This methodology was introduced by Srnec and co-workers and is referred to as variable-temperature H-Atom addition/abstraction (VT-HAA)[75].

The gold standard using DFT or wavefunction based methods, is still a completely atomistic description of the solvent. Sprik and co-workers developed a DFT-MD and free energy perturbation scheme based protocol that allows the calculation of reduction potentials and pK_a values[76]. A complete rehearsal of this method would be beyond the scope of this work, therefore we will only introduce the fundamental concept (for a more detailed description see Refs.:[77–81]). The scheme has strong ties to Marcus theory[82] and is conceptually based on the calculation of the free energy of insertion of an electron or proton into the simulation box. The latter is done by a thermodynamic integration scheme of the vertical energy gap between the two states (with and without an electron or proton respectively). In practice this means that not only the initial state and final state, but also intermediate states have to be sampled, in order to calculate the pK_a or reduction potential of a certain species. This is in particular true for the insertion of a proton where the solvent response is non-linear. Due to the requirement of a reference state within the same methodology and in particular within the same simulation box, a computational hydrogen electrode ($H_2 \longrightarrow 2\,H^+ + 2\,e^-$) has to be calculated as well. AIMD simulations are usually performed employing generalized gradient approximation (GGA) exchange-correlation functionals, which are known to perform worse in terms of energy differences than hybrid functionals. However, due to the high computational cost the use of hybrid functionals for MD simulations is currently often out of the question. It is therefore recommended to recalculate the vertical energy gap employing a hybrid functional. The latter adds even more cost to an already expensive methodology, which in fact limits its applicability to small systems.

In case neither reduction potentials or pK_a values are of interest but rather dehydrogenation free energies i.e. the free energy difference of a PCET, then certain shortcuts can be taken since there is no need to calculate the computa-

tional hydrogen electrode, which makes the protocol more affordable. But why should one be interested in PCETs instead of reduction potentials and pK_a values? Every water oxidation mechanism can be formulated as sequence of four PCETs in order to avoid the accumulation of charge which presumably leads to high energy intermediates. Recently we successfully applied the above mentioned protocol to calculate dehydrogenation free energies for a model system of a transition-metal based WOC, a solvated Co(II)-ion, and thereby shown that in the future this methodology might become viable to investigate transition metal catalyzed water oxidation[83].

With this general introduction on transition metal catalyzed water oxidation we laid the foundation for the following sections, where we will highlight selected contributions made by Luber and co-workers in the context of water oxidation. In the last few paragraphs we put special attention on some aspects of the modeling process, which later in the discussion of the catalytic systems will reoccur. Thereby we aimed neither to give a full scope of all available methods and protocols nor to give an in-depth description of presented ones. The sole purpose was to give the reader an insight into the methodology used by ourselves and set it into the context of the field.

3. Bioinspired Cobalt Based Water Oxidation Catalysts

3.1. The Cubane Structure in Co-based WOCs

In the following section we discuss the joint efforts made by Patzke, Luber and co-workers in developing and understanding Co(II)-cubanes that are active water oxidation catalysts (see Fig. 5). It is not a coincidence that we have chosen to work on those structurally rather complex WOCs. Nature itself uses a cuboidal transition metal cluster known as oxygen-evolving-complex (OEC) to perform water oxidation. The latter is embedded into a huge protein complex, the photosystem II (PSII), located in the thylakoid membrane of chloroplasts. The cluster itself is composed of calcium and manganese cations bridged by oxygen atoms $\{CaMn_4O_5\}$ The fourth manganese cation, which is referred to as

the dangling manganese, is located outside of the cubane core that is composed of $CaMn_3O_4$ [84]. Until now, the mechanism for water oxidation catalyzed by the OEC is still under debate[85–93]. Even though many attempts have been made to synthesize $CaMn_xO_x$ clusters that mimic the structure of the OEC, so far none of them is able to oxidize water catalytically[94–98]. However the cubodial core structure has also served as an inspiration for the design of artificial WOCs that are not based on manganese such as for example cobalt-based cubanes[43,99,100]

[Figure 3 about here.]

Among those bio-inspired WOCs are the previously mentioned Co(II)-cubanes, that are not only unique in taking advantage of the lower oxidation state of cobalt (II instead of the usual III), which goes along with a more flexible ligand sphere i.e. faster ligand-exchange reaction rates, but also the use of ligands such as pyMeO = pyridin-2-ylmethanloate or dpyC(OH)(O) = hydroxyldi-2-pyridinylmethanolato (see Fig. 3). The latter not only coordinate the metal centers but are an integral part of the Co_4O_4 core[43,100]. The covalent linkage of the bridging oxygen to the ligands renders dissociation reactions highly unlikely. The linkage further prevents the bridging oxygen atoms from being protonated to participate in the oxygen-oxygen bond formation, which has been considered for model systems of Co_xO_3, where a $\{Co(III)_4O_4\}$ cubane core is coordinated by aqua and hydroxido ligands[101–104]. We reviewed the mechanistic studies of those model systems in detail in Ref. [10] and will therefore not discuss them in detail.

The main problem with Co(III)-cubanes is their unknown structure in solution. Depending on the level of theory, and especially the solvation model applied, huge differences in the stability of the large number of protomers can be observed. This in turn renders different reaction mechanisms and / or different intermediates energetically feasible or not. Beside the model systems for Cobalt-oxide WOCs there exists only one homogeneous WOC featuring a Co(III) based cuboidal core, $\{Co(III)_4O_4\}$ ($[Co^{III}{}_4(\mu^3\text{-}O)_4(\mu^2\text{-}OAc)_4(Py)_4]$, OAc = acetate, py = pyridine) which is often referred to as Dismukes-cubane[99]. Since those

cubanes do not possess an aqua ligand, in a first step an acetate ligand has to change its coordination mode from μ^2 to μ^1 in order to allow the coordination of a water molecule[103,105–107]. This substitution reaction is expected to take place after a first oxidation of the catalyst, and is followed by the deprotonation of the newly formed aqua ligand. This species might be part of the actual water oxidation cycle, however some authors argue that the experimentally supplied oxidation potential was not large enough to reach the later intermediates of the catalytic cycle[105,107]. Therefore, they proposed the association of a second hydroxide or water ligand to the cubane core with or without displacement of an acetate ligand. The existence of a dihydroxo species $\{Co(III)_4O_4(OH)_2\}^-$ has been proven experimentally, yet considerations from thermodynamics led to the non-substituted species $\{Co(III)_4O_4\}$ being strongly favored[106].

It has also been shown that $\{Co(III)_4O_4\}$ can be chemically oxidized to $\{Co(III)_3Co(IV)O_4\}^+$, the latter has been isolated and was fully characterized. Due to the elusive nature of catalytic intermediates, their isolation and in-depth study tend to be very challenging. The oxidized species $\{Co(III)_3Co(IV)O_4\}^+$ was the basis for a wide range of kinetic and mechanistic studies. The most astonishing observation thereby was that $\{Co(III)_3Co(IV)O_4\}^+$ was found to evolve O_2 without the need of an additional oxidant, upon dissolution in basic aqueous media. From this Nguyen *et al.* concluded that $\{Co(III)_4O_4\}$ might disproportionate into $\{Co(III)_3Co(V)O_4\}^{2+}$ or $\{Co(III)_2Co(IV)_2O_4\}^{2+}$, since the existence of a formal Co(V)=O has been thought of to be a prerequisite for water oxidation[106]. The ability of polynuclear transition metal complexes to disproportionate in order to reach high oxidation states was recently also recognized in a novel proposal for the water oxidation mechanism by the nature's OEC[108]. In their latest study Nguyen *et al.* modified both the pyridine and the acetate ligands in order to alter the electronic properties of the cubane. The collected experimental data allowed them to derive an empirical (and specific to this kind of cubane) formula to predict reduction potentials of possible catalytic intermediates[107]. Using this tool, they were able to revise their reaction mechanism proposed earlier. Their current mechanistic proposal suggests an

active species with two hydroxido ligands in a *syn* configuration, as opposed to their previous active species which contained only one hydroxido ligand. The *syn* alignment of the hydroxido ligands renders an intramolecular reaction more feasible (i-WNA(OH)) than the earlier suggested intermolecular pathway where the O−O bond formation proceeds through a $WNA(OH_2)$/WNA(OH) (see Fig. 2). The latter is supported by recent *in situ* XAS measurements performed by Brodsky *et al.*, that provided the evidence for the existence of $\{Co(III)_2Co(IV)_2O_4\}^{2+}$ [109]. This structure in principle, also allows for an O−O bond formation by an intramolecular RC (I2M) mechanism.

To summarize the studies on Co(III)-cubanes, there are some theoretical studies on $\{Co_4O_4\}$ cores featuring only aqua and hydroxido ligands[102–104,110]. Results from those studies are difficult to generalize since the different protocols favor different protomers. However these studies represent a great example on how complex even 'simple' model systems tend to become if one attempts to consider all their aspects. The Dismukes-cubane was studied in great detail from an experimental and computational point of view. Despite the complexity of the system, the combination of both experimental and theoretical work led to a steady improvement of the proposed catalytic cycles. The extensive studies also revealed, that some of the early synthetic protocols suffered from Co(II) impurities, which were responsible for some of the catalytic activity. The problem was overcome by the introduction of an additional purification step in the synthetic protocol[111,112]. The observation that impurities can also contribute significantly to the overall catalytic performance highlights the importance of in-depth studies of the catalysts speciation in solution, as well as its stability.

[Figure 4 about here.]

3.2. Discovery of Co(II) Cubanes

The first Co(II)-based cubodial water oxidation catalyst $[Co^{II}{}_4(pyMeO)_4(\mu\text{-}OAc)_2(\mu^2\text{-}OAc)_2(H_2O)_2]$ (pyMeO = pyridin-2-ylmethanolato) $\{Co_4(pyMeO)_4\}$ was discovered by Evangelisti *et al.*[100]. The turn-over-number

(TON) was found to be similar to that of the Co(III) cubanes while the turn-over-frequency (TOF) was determined to be two orders of magnitude higher. The catalytic performance was found to be pH dependent, employing mildly basic conditions (pH = 8) and resulted in highest TON, while even more basic conditions i.e. pH = 9 gave the highest TOF values. Those observations were in agreement with the spectroscopically determined pK_a value of the aqua-ligand of 8.7, indicating that at high pH values the aqua-ligand is already deprotonated. A secondary pK_a was found at 5.8 which was attributed to a potential substitution of an OAc ligand.

Being aware of the issue of Co(II) impurities in the case of Co(III)-cubanes, this led to several experiments being conducted in order to exclude Co(II)-leaching[100].

Isolation or characterization of elusive catalytic intermediates had turned out to be impossible, in particular for photocatalytic water oxidation where there are many other components in solution (e.g. buffer ions, persulfate ions, and photosensitizers). Based on previous studies on similar polynuclear catalysts such as for example the work by Piccinin *et al.*[113], we carried out a theoretical study to elucidate possible mechanisms governing water oxidation catalyzed by $\{Co_4(pyMeO)_4\}$[114].

[Figure 5 about here.]

Water Nucleophilic Attack Mechanism

The structural features of $\{Co_4(pyMeO)_4\}$, where a cobalt-center is coordinated by an aqua ligand, strongly suggest a WNA mechanism - in case the ligand sphere remains intact upon dissolution of the WOC. Such a mechanism would in essence be a single-site mechanism where the other three cobalt-centers act as spectators. Because the spin-state of the active cobalt is not known during the catalytic cycle, geometry optimizations for all reasonable possibilities had to be performed. We found not only the single-site hypothesis confirmed, i.e. the other three metal centers remained in a high spin state of Co(II) (S = 3/2,

where S is the total spin angular momentum), but we also observed a surprising consistency in terms of the energetically favored spin state among different functionals, namely the GGA functional BP86[115,116], and the hybrid functional B3LYP[117,118], different program packages CP2K[119] and Turbomole[120] as well as different solvation models (implicit (COSMO)[121] and explicit).

[Figure 6 about here.]

As a first step, the thermodynamics of the proposed catalytic cycle, composed of four PCETs and a WNA, were evaluated (see Fig. 1). The largest difference in terms of free energy between two states was found to be the transition from S2 to S3. The latter includes the O – O bond formation by a WNA, as well as a consecutive PCET forming a hydroperoxo species (S3).

In order to release molecular oxygen, the species has to be oxidatively activated i.e. it has to undergo a further ET and PT reaction. Based on the experimental conditions, i.e. a huge excess oxidant and base, we assumed all the ET, PT or PCET steps to be barrierless. Further, instead of a water molecule, a hydroxide might could have been the nucleophile, however the maximum catalytic performance at a pH of 8 suggested otherwise.

Thermodynamics can only give an incomplete picture of the catalytic cycle, barriers for the O – O bond formation as well as for the O_2 release were therefore calculated as well. For those reactions water is not only the solvent but also the substrate, therefore its interactions with the catalyst cannot be neglected. This is why our model contained a full first solvation shell, the structure of which was obtained from AIMD. To be consistent, not only the barriers but also the thermodynamics were calculated for a explicitly solvated catalyst. The barriers were obtained by climbing image nudged-elastic-band (CI-NEB) calculations[45,46]. This protocol relays on the premise that reaction is a sole rearrangement of chemical bonds, i.e. the number of electrons and protons in the system remains the same. In the case of the O – O bond formation, this means that besides the Co(III) – OOH species a H_3O^+ also has to be formed. Even though we used a generous first solvation shell, stabilization of a cation in

close proximity to the catalyst appeared to be energetically unfavorable. Note that this intermediate was not considered when evaluating the thermodynamics, since in this case we combined the WNA with a PCET in one step. The calculated value of the barrier is due to the reasons discussed above probably an overestimate of the 'true' barrier, nevertheless the CI-NEB intermediates allowed us to study how different orbitals are involved in the bond formation mechanism. Of particular interest are the unoccupied σ^* and π^* orbitals at the oxo-ligand, which we identified to be detrimental for a WNA.

The same procedure was used to determine the barrier for the substitution of metal bound O_2 by solvent molecule. While this reaction in principle is only a rearrangement of chemical bonds, it proceeds with change of the preferred spin state. Since the catalyst is expected to evolve triplet oxygen, the spin state of the system after the reaction should be S = 7 ($4 \cdot 3/2$ Co(II) + 2/2 O_2), while for the S4 state we found S = 5 ($3 \cdot 3/2$ Co(II) + 1/2 Co–OO) to be the thermodynamically most stable one. As a consequence the barrier from CI-NEB calculations might also be an overestimate, however since it was found to be significantly lower than O–O barrier we concluded that it is not rate-determining.

Ligand Exchange and the Influence of Buffer Molecules

As mentioned earlier, there is also the possibility that an acetate ligand is substituted by a water or hydroxide molecule, or that it changes its coordination mode from bidentate to monodentate upon association of a solvent molecule. In case such reactions were feasible, several alternative reaction pathways would become possible.

In order to assess the energetics of cubanes with a slightly modified coordination sphere, we performed a series of AIMD simulations, where we used a simulation box containing the cubane ($\{Co_4(pyMeO)_4\}$) and 190 water molecules[43]. For each reaction we equilibrated the reactant, and the product - for example: $\{Co_4(pyMeO)_4\}$ + OH^- in the box of 190 water molecules respectively $\{Co_4(pyMeO)_4(OH)\}$ + OAc^-, where OAc^- was previously coordinated to the

'active' cobalt center in a monodentate fashion. In the context of solvation models, we refer to AIMD simulations as an explicit dynamic solvation. Those reaction energies were then compared with those obtained by implicit, and static explicit solvation. With static explicit, we refer to geometry optimizations of the cubane including several water molecules, the limit of which we tested by including a complete first solvation shell composed of 68 water molecules. In contrast to this, implicit solvation refers to the application of COSMO or COSMO-RS to the cubane only.

Employing AIMD, we found all reaction energies where the reactant was $\{Co_4(pyMeO)_4\}$ to be endothermic, while they have been found to be approximately isoenergtic in the case of $\{Co_4(pyMeO)_4(OH)\}$. This indicates that both species could co-exist in solution. Reaction energies for static explicit solvation were obtained from optimizing three different solvation shells, which were extracted from the AIMD trajectories.

Among the three reaction energies, we observed a spread of 5-20 kcal/mol, that indicated that local changes in the solvation shell had a significant influence. Nevertheless, there was an agreement with the overall trend observed for the reaction energies obtained by AIMD. Exceptions were the reaction energies of the water association to $\{Co_4(pyMeO)_4\}-OH$, where the spread of the reaction energies was too large in order to make a definite conclusion. Reaction energies obtained by implicit solvation i.e. COSMO, rendered all reactions feasible, in contrast to reaction free energies calculated using COSMO-RS. The latter were qualitatively in agreement with the results of the AIMD simulations and gave rise to endothermic or isoenergetic reaction energies.

Comparing the different solvation models clearly showed that static explicit solvation should not be used to calculate reaction energies if the underlying reaction proceeds with a severe change of the solvation shell. The latter is in particular true for substitution reactions. On the other hand, PCET reactions, which are an integral part of any water oxidation mechanism, are not expected to cause significant changes to the solvation shell as long as the proton is not transferred to a solvent molecule but rather 'removed' from the simulation box.

This was further highlighted by the fact that shrinking of the explicit solvation shell i.e. deletion of solvent molecules, no matter whether close or far away from the 'reactive site', led to severe changes in the reaction energy. The rationale behind this is simple, optimizing the structure of the solvation shell led to a fixed set of hydrogen bonding interactions. The latter have to rearrange upon removal of a participant, which in turn can lead to different local minima. The differences between COSMO and COSMO-RS might in part be caused by hydrogen bonding which is not explicitly accounted for in standard implicit solvation models. However for complex systems such as $\{Co_4(pyMeO)_4\}-OH$, there are several possibilities how the solvent can interact with the ligand sphere and thereby stabilize certain conformations.

Moving from a purely thermodynamical point of view to a kinetic one, we were interested in estimates of the reaction barriers as well. We employed the CI-NEB methodology (without explicit solvation) to calculate the reaction barriers for the substitution of an acetate ligand of $\{Co_4(pyMeO)_4\}$ by either a hydroxide or a water molecule. All barriers obtained using this approach turned out to be far from reasonable, since the solvent played a crucial role in stabilizing not only the intermediates but also the associated reactant, i.e. the state where the reactant and the substrate are in close proximity. We therefore turned our attention towards an enhanced sampling method which is suited for a fully solvated system, metadynamics. During the course of 49 ps we observed a step-wise reaction, where first an intramolecular hydrogen bond between the acetate ligand and the aqua ligand was replaced by an interaction with the solvent. Then, the Co–OAc bond was elongated and finally broken, the now free OAc engaged in a hydrogen bond with the aqua ligand (see Fig. 6). This simulation undoubtedly has shown how complex solute-solvent interactions are in terms of their constantly adapting hydrogen bonding network. An important drawback is the computational cost that is usually very high. Moreover, one has to know beforehand which components of the reaction coordinate to be subjected to a bias potential. This task is often not trivial and requires a lot of trials. Summarizing we have clearly shown, that explicit solvation, in particular

in a dynamic approach, is crucial for systems when there are flexible directed interactions e.g. hydrogen bonds between the solute and substrate. In some cases, in particular when only interested in thermochemistry, then the use of implicit solvation might be preferred over more extensive static and dynamic explicit solvation shells.

Another interesting aspect of the system at hand is its dependence on the pH and the respective buffer ions. In order to determine whether coordination of the latter to the cubane is energetically favorable, we performed AIMD simulations. While coordination of borate was found to be endothermic independent of the coordination mode, a bidentate coordination of phosphate was found to be energetically favorable. Those observations suggested that a significant amount of the catalyst might be trapped in unproductive states in phosphate buffer where a buffer ion coordinates to the cubane. The latter is in agreement with the significantly lower catalytic performance in phosphate buffer compared to borate buffer[100].

Radical Coupling Mechanism

Our extensive study on ligand substitutions in the first solvation shell suggested that $\{Co_4(pyMeO)_4(H_2O)\}^+$ ($[Co^{II}{}_4(pyMeO)_4(\mu\text{-}OAc)(\mu^2\text{-}OAc)_2(H_2O)_3]^+$), where a monodentate acetate is replaced by a solvent molecule exists under reaction conditions.

For $\{Co_4(pyMeO)_4(H_2O)\}^+$ there are several alternative routes for the O–O bond formation, among them is an intramolecular RC after four consecutive PCETs (see Fig. 1), and an intermolecular WNA at the same stage.

In the following we will focus on the RC mechanism, for which different spin states as in the case of the single site mechanism were in principle possible. When employing different programs, functionals and solvation models the relative stability of those spin-states was less consistent as compared to that of the single-site mechanism. Looking at the thermodynamics, we found the first two PCETs to be more demanding in terms of free energy compared to the corresponding ones of the WNA mechanism, i.e. the formation of the first

metal oxo required more energy. This can be rationalized by comparing the overall charge of the catalyst, that is higher due to an exchange of an anionic ligand by a neutral one, which in turn renders oxidations more challenging. In contrast to the WNA mechanism, reaching the S3 state, which is different for the two mechanisms i.e. {Co(III)−OOH} vs {Co(III)−OH}, {Co(IV)=O} and the subsequent dioxo state (S4) was calculated to be more feasible. Barriers for the O−O formation and the O_2 release, which in this case were both just rearrangements of chemical bonds, were investigated in a single CI-NEB. We found that, directly after the RC bond formation, the bridging O_2 was substituted by a water molecule from the solution, resulting in *endo*-coordinated O_2, which was found to be a stable intermediate. In a secondary reaction, O_2 was then released from the catalyst and its ground state was regenerated by the uptake of an additional water molecule. The barriers for the RC mechanism were determined to be significantly lower than the one for the WNA, and show the same trend, that the O−O bond formation is rate-determining.

Based upon our results we have made some suggestions how to improve the catalytic behavior of $\{Co_4(pyMeO)_4\}$ such as for example how ligands might be modified to lead to a more flexible ligand shell and a lowering of the barriers of the O−O bond formation and O_2 evolution[114].

3.3. Co(II)-Lanthanide Cubanes

The second generation of Co(II) based cubanes features the same ligand as the first one, however they include a redox-inert lanthanide ion $\{Co_3Ln(pyMeO)_4\}$ ($[Co^{II}{}_3Ln(pyMeO)_4(\mu^2\text{-}OAc)_4(\mu\text{-}OAc)H_2O]$, Ln = Er, Tm, Yb, Ho) (see Fig. 5)[43]. The catalytic performance of the latter is significantly improved compared to $\{Co_4(pyMeO)_4\}$. This is surprising, in particular since the redox-inert lanthanide ion is not expected to directly participate in the water oxidation mechanism. As for $\{Co_4(pyMeO)_4\}$, the catalytic performance was found to be strongly dependent on pH and the buffer media. The best performance was usually measured under mildly basic conditions (pH = 8). It further has been shown that the aqua-ligand undergoes rapid exchange with solvent molecules,

and the acetate ligands do to some extend. This left us with the question - what is the structure of the active species of the catalyst?

In a first step, we determined the structure of the catalyst in solution, where we limited ourselves to two out of the four lanthanide cations in the cubane core: Erbium which resides at the top in terms of catalytic performance and Thulium, which covers the lower end. AIMD simulations revealed that, in contrast to $\{Co_4(pyMeO)_4\}$, for $\{Co_3Ln(pyMeO)_4\}$ (Ln = Er, Tm) the displacement of bidentate acetate molecules by solvent molecules is thermodynamically favorable. Further, the displacement of a monodentate acetate coordinating the active cobalt center by a water ligand (Co(II)$-H_2O$) as well as the substitution of both bidentate acetate ligands bound to the lanthanide by a hydroxide molecule turned out to be energetically feasible. Analogous observations were also made in static calculations employing implicit solvation. This led to the assumption that the dominant species in solution is $[Co^{II}{}_3Ln(pyMeO)_4(\mu^2\text{-}OAc)_2(OH)_3H_2O]$, rather than the pristine crystal structure[43,67].

As in the case of $\{Co_4(pyMeO)_4\}$, the stability of the WOC in solution before and after catalysis was studied throughly by a wide range of experimental techniques, all of which provided supporting evidence for the catalysts robustness[67].

Possible Water Oxidation Pathways

Having established the catalytic resting state, we further explored the thermodynamics and kinetics of the water oxidation mechanism. Thereby we applied the same protocol as already successfully applied for $\{Co_4(pyMeO)_4\}$[100,114]. In the catalytic ground state only one cobalt center bears an aqua ligand, and we refer to the latter as the active cobalt center. The fact that there is only one aqua ligand suggests that a single-site mechanism governs the water oxidation reaction. The active cobalt is further coordinated by a hydroxido ligand in a geminal alignment with respect to the aqua ligand. This in principle allows for two reaction pathways, where the Co(IV)=O is either on the same face of the

cube as the erbium ion (pathway A) or on a different one (pathway B) (see Fig. 7).

[Figure 7 about here.]

We compared the thermodynamics of the two reaction pathways obtained using explicit solvation. The free energy difference for the S1-S2 transition was found to be marginally larger for pathway B in the case of $\{Co_3Er(pyMeO)_4\}$, and significantly lower in the case of $\{Co_3Tm(pyMeO)_4\}$[67]. This was attributed to a distortion of the cubane core, caused by the active cobalt-atom which is slightly pulled out of the cubane cage upon reaching the S2 state. This opening appeared to be thermodynamically favorable, and we observed it to some extent independent of the reaction pathway (A or B) for both lanthanide cubanes. However, we only found such distortions when employing explicit solvation. This indicates significant interactions between the first solvation shell and cubane core which cannot be accounted for by an implicit solvation model. Independent of the opposing behavior in terms of energetics, pathway B was found to be favorable for both catalysts in the case of explicit solvation. Applying implicit solvation resulted in smaller free energy differences for all catalytic steps. Again pathway B was found to be thermodynamically favored, however to a lesser degree than with explicit solvation.

Minimum energy pathways for the O – O bond formation were again obtained by employing CI-NEB calculations, the limitations of which were discussed earlier (see Fig. 8)[67]. In contrast to $\{Co_4(pyMeO)_4\}$ we found some of the hydroxido ligands of $\{Co_3Ln(pyMeO)_4\}$ to be spontaneously protonated during the O – O bond formation. This is in particular true for the erbium bound hydroxido ligands (only for pathway A). Protonation of the latter inhibits the formation of a hydronium ion in close proximity, which is directly translated into a lower activation barrier.

While in principle the nature of the lanthanide cation was found to have only a minimal influence upon the structures and therefore the energies of the reaction, there was still one major difference between $\{Co_3Tm(pyMeO)_4\}$ and

$\{Co_3Er(pyMeO)_4\}$. In the case the of former the S2 state was calculated to be more stable than the one of $\{Co_3Er(pyMeO)_4\}$. In this state the active cobalt center was slightly pulled out of the Ln-distorted cubane. The accepting orbitals - i.e. the unoccupied orbitals which are prone to a nucleophilic attack by the water molecule - play a crucial role in the WNA mechanism. For the distorted cubane we found that in particular the σ^* orbital of the Co(IV)=O became partially occupied, which renders a WNA unlikely. This is reflected by our calculations where we found a higher barrier for the O−O bond formation. The partial occupation of the accepting orbital became possible due to redox-isomerism inside the cubane core. In this case, one of the spectator cobalt centers was formally reducing the active cobalt. The latter highlights the role of the cubane core in the reaction mechanism which goes beyond a simple structural framework.

The distorted cubane core was also observed for $\{Co_3Er(pyMeO)_4\}$, however to a less extent. Simultaneous with the O−O bond formation, the distortion of the cubane core reverted and the Co−O bonds returned to their initial length. For pathway B we did not observe the protonation of erbium hydroxido ligand, instead a hydronium ion was formed apart from the cubane. Further a hydroxido ligand of the active cobalt was protonated by a solvent molecule, forming a hydroxide in close proximity to the catalyst. Stabilization of those two charged species is difficult, in particular with a limited solvation shell. Therefore the barriers for pathway B were significantly larger than the one for pathway A, independent of the lanthanide ion.

To summarize, on one hand thermodynamics favor pathway B where the active ligand is not on the same face of the cubane as the lanthanide ion. On the other hand, kinetics strongly favor pathway A. The rationale behind this is the avoidance of the formation of an energetically unfavorable hydronium during the WNA in pathway A. As for $\{Co_4(pyMeO)_4\}$, there is currently no experimental data available which would allow to distinguish between the two pathways presented here.

[Figure 8 about here.]

Opening of the Co(II)-Lanthanide Cubane Cage

The existence of intermediates featuring a distorted cubane core, led to an extensive study with the aim to verify whether there might exist an alternative reaction pathway[122]. Inspired by those distorted cubanes, we identified structures where the active cobalt center is even further pulled out of the cubane core. We will refer to those structures as 'open' (see Fig. 9). In fact, the active cobalt center obtains a tetrahedral coordination as opposed to an octahedral one as in the case of the 'closed' cubane. Further, one of its ligands forms an intramolecular hydrogen bond with the alkoxide of the neighboring ligand, thereby stabilizing the 'open' form. This is of course only possible for pathway B, where the active ligand is not on the same face of the cubane as the lanthanide ion.

We located those 'open' cubane structures for both lanthanide ions, employing either implicit solvation or explicit solvation, for all proposed intermediates of the catalytic cycle (S0 to S4). Employing implicit solvation we determined for both catalysts the 'open' form of the S0 state to be slightly favored in terms of free energy, while the two forms are isoenergetic in the S1 state. For the S2 state, which is of great importance for the reactivity of the catalyst, we found $\{Co_3Er(pyMeO)_4\}$ to prefer an 'open' configuration while $\{Co_3Tm(pyMeO)_4\}$ favors 'closed' configuration. Intermediates of the subsequent states favor a 'closed' form. The latter are further stabilized by an additional intramolecular hydrogen bond between the hydroperoxide and the hydroxido ligand of the active cobalt center. Looking at thermodynamics of the whole catalytic cycle we found no overall benefit of an all 'open' vs. an all 'closed' cycle. Due to the close energetics of those two forms in the S0 and S1 states, we calculated the barrier of the interconversion (open-closed) to address the question whether the two species might co-exist. The approximated barrier of this transition was obtained by self-consistent optimization of the reaction path[44]. The height of the latter was small (< 6 kcal/mol), thus rendering the transition possible.

Therefore, the open form of the cubane might only play a role for some states of the catalytic cycle. This is to some extent reminiscent of one of the proposed catalytic mechanisms of the OEC, where the cubane core possesses both an 'open' and a 'closed' form in the S2 state. The 'open' form is then suspected to undergo a further PCET to reach the S3 state[123]. The final steps of the cycle, including the O – O formation are still under debate[108].

[Figure 9 about here.]

Keeping in mind the limits of implicit solvation models in terms of describing directed solute-solvent interactions, we employed direct COSMO for real solvents (DCOSMO-RS), to our model system as well. In the DCOSMO-RS formulation the free energy of solvation of COSMO-RS is converted to a Fock-matrix contribution, which allows to account for contributions caused by the response of the solute due to solvation[59]. For most intermediates the difference between COSMO and DCOSMO-RS was found to be minimal. However, in the case of the S2 state, we found significantly lower free energies using DCOSMO-RS, and the latter was consistent with an increased polarization of the COSMO shell in close proximity of the oxo-ligand. This points towards the hydrophilic nature of the oxo-ligand, which in turn suggests its involvement in hydrogen bonding or at least its ability to strongly polarize and therefore re-orient the solvent molecules in close proximity. Indeed, we found the solvent molecules to engage in hydrogen bonding with the oxo-ligand using explicit solvation[67,114]. Further, employing explicit static solvation we found the open structure to be energetically favored throughout the catalytic cycle. Comparing the 'open' and 'closed' cubane structures with and without explicit solvation we were able to verify that intermediates S0 and S1 indeed favor an 'open' configuration while the stabilization of the later intermediates was attributed to changes in the solvation shell. The fact that there are many different energetic minima with respect to the solvation shell makes the calculation of energy differences between catalytic intermediates somewhat arbitrary. The reason for this is due to the fact that it is uncertain whether the energy difference is caused by the change of

the solute or primarily by a structural change of the solvent shell, which might occur independent of the solute[54]. The introduction of many explicit solvent molecules into the simulation box thus in principle requires the use of sampling techniques such as molecular dynamics.

3.4. A New Generation of Co(II) Cubanes

We tackled this problem in our latest study on Co(II) based cubanes i.e. $[Co^{II}{}_4((dpyC(OH)(O))_4)(OAc)_2(H_2O)_2]^{2+}$ (dpyC(OH)(O) = hydroxy-di(pyridin-2-yl)methanolato, $\{Co_4(dpyC(OH)(O))_4\}$) (see Fig. 3)[124]. The latter represents the third generation of cubanes developed by Patzke and co-workers. A major difference compared to the previous generations is the use of a tridentate ligand, instead of the bidentate one used before. The novel ligand might be thought of as an extended version of pyMeO, where the methylene hydrogen atoms were replaced by a pyridine and a hydroxide. The similarity to the previous ligand pyMeO was intended in order to take advantage of the favorable properties observed for $\{Co_4(pyMeO)_4\}$ and $\{Co_3Ln(pyMeO)_4\}$, such as the incorporation of the ligand into the cubane core, which prevents the bridging oxygens from participation in the water oxidation mechanism. The $\{Co_4(dpyC(OH)(O))_4\}$ cubanes are not only interesting from a mechanistic point of view, but they also possess another key feature unknown for the other cubanes; it is experimentally possible to stoichiometrically replace Co(II) by Ni(II), while keeping the same structure. This potentially allows for unprecedented insight into the catalytic mechanism, in particular on how the nature of the transition metal might alter its kinetics and/or thermodynamics.

There is another important structural feature: For the first time two aqua ligands are located on the same face of the cubane. Together with the non-coordinating hydroxyl group of the ligands, they form an edge-site which strongly resembles the solvated surface of Co_xO_3. This makes $\{Co_4(dpyC(OH)(O))_4\}$ the ideal model system to study both homogeneous and heterogeneous reaction mechanisms for water oxidation, although the catalytic performance was found to be slightly worse than the previous generations (TON: 20, TOF $0.24s^{-1}$)[124].

Those two aqua ligands have a crucial impact on the possible reaction mechanism. Since these ligands are coordinated to metal centers with the same chemical environment, it is likely that both of them are involved in the water oxidation mechanism. Thereby it remains unknown whether the reaction follows a WNA(i-B assisted), i-WNA(OH) or an i-RC pathway to form the O–O bond (see Fig. 2). In contrast to this, for the previous generations of cubanes we generally assumed a single-site mechanism unless a second water molecule is expected to associate to the cubane core[67,114].

Experimentally it turned out to be difficult to characterize catalytic intermediates. However, recording X-ray absorption near edge structure (XANES) under catalytic conditions revealed the partial oxidation of the cubane and its slow recovery to the catalytic ground state, i.e. the complete reduction to an all Co(II) state. Even though those experiments cannot give an insight into the reaction mechanism, at least they strongly support the claim that the catalyst is stable under catalytic conditions.

As a prerequisite for the proposal of a possible reaction mechanism, the species in solution had to be determined. Based on our previous studies[54,67,114] we chose to explicitly solvate the cubane by either 208 or 452 water molecules. Being curious about the discovery of the 'open' structures for $\{Co_3Ln(pyMeO)_4\}$, we therefore monitored the Co–Co distances as well as the volume enclosed by the cubane cage during the AIMD runs. While we observed significant fluctuations of all Co–Co distances, some of which appear to be correlated, we did not detect an opening of the cubane cage, probably due to restricting factors introduced by the bigger ligands which hold the cobalt ions in place. Since the highest catalytic activity was observed under mildly basic conditions (pH = 8.5), which is also the sole experimentally determined pK_a value of the WOC, we also checked whether the other functional groups of the 'edge-site' could engage in proton transfer reactions. Modeling of a deprotonated cubane ($[Co^{II}_4((dpyC(OH)(O))_4)(OAc)_2(H_2O)(OH)]^+$) revealed the involvement of not only the ligands and the solvent in various proton transfer reactions, resulting in deprotonation of the hydroxyl group of a ligand in favor of the aqua ligand. This

study highlights the importance of an appropriate solvation model, as already pointed out by us in our previous studies on Co(II) cubanes. At the same time it also complicates the proposal of a catalytic mechanism, since there are many protomers for each intermediate. Further investigations are currently ongoing in our group.

4. Mononuclear Ru-based Water Oxidation Catalysts

Noble metals such as ruthenium have been widely used in catalysts for water oxidation, especially because the first discovered molecular water oxidation catalyst, the so called 'blue-dimer', already contained ruthenium[125,126]. Since then there have been numerous publications on different catalysts and their possible mechanisms. A full review of the field is beyond the scope of this work, therefore we want to point the reader's attention towards some important reviews such as Refs.[19,127–132]. In the following sections we will primarily focus on work done by our group. However, we put our work into a broader context, in order to embed our contribution into the work of others in this field.

4.1. Ru-WOCs based on the bda Ligand

Ru-based WOCs featuring a bda (2,2′-bipyridine-6,6′-dicarboxylic acid) ligand have been studied by various groups. For instance Tong *et al.* were able to show in a combined experimental and theoretical study how introducing rigidity into the ligand, i.e. the usage of pda (phenantroline-2,9-dicarboxylic acid) instead of bda, led to a different reaction mechanism for the O−O bond formation (see Fig. 10)[40]. While the flexible bda ligand favored an oxo-oxo coupling pathway, the rigid pda ligand preferred a WNA mechanism. However, altering the reaction mechanism had a profound effect on the catalytic performance. The latter was in the case of the pda WOC significantly lower than the one of the bda containing catalyst in terms of TONs i.e. 310 vs 1200 for $[Ru(L)(pic)_2]$ (where L is pda rsp. bda). Despite the lower TONs an enhanced lifetime of pda bearing catalysts was observed. However, it remains unclear whether the

increased lifetime is directly translated into an enhanced stability or if the water oxidation reaction itself is just slowed down. In an attempt to rationalize the effect of the rigidity, the reorganization energy of the ligand was calculated i.e. the energy difference required to deform the free (non coordinated) ligand towards its geometry, when coordinated to the metal center[40]. Independent of the oxidation state of the metal center, the reorganization energy remained the same for the pda ligand, while for the bda ligand drastic changes (up to 10 kcal/mol) were observed. This highlights the fact that the bda ligand can adopt to the smaller ionic radii of the higher oxidation states while there is a growing mismatch between the pda ligand and the metal ion upon oxidation.

Taking all those observation into account, our experimental co-workers in the groups of Alberto and Llobet came up with a ligand which in essence is the exact opposite of the pda ligand. Instead of locking the bipyridine subunit into one plane, they enforced non-planarity by replacing pyridine by isoquinoline resulting in biqa ([1,1′-biisoquinoline]-3,3′-dicarboxylic acid)[41] (see Figure 10). While this ligand can in principle rotate along its 1,1′-bond and therefore adopt to changing ionic radii easily, there is a significant penalty associated in case the dihedral angle describing the alignment of the two isoquinoline subunits approaches small values, i.e. planarity. To complete the catalyst, they incorporated picoline (pic) and 6-bromoisoquinoline (isoq) as axial ligands. The rational behind this is an outstanding study on Ru-bda WOCs by Duan *et al.* where they reported a drastic increase in catalytic performance upon replacing pic with isoq, in particular the TOF increased by almost an order of magnitude ($303\ s^{-1}$ compared to $32\ s^{-1}$)[133]. The reason for this increase is suspected to be the favorable interaction of the axial ligands in the I2M mechanism, stabilizing either the encounter complex or the transition state. Elucidating the influence of the axial ligands has since then received a lot of attention, and several groups tried to explain its nature from both an experimental and theoretical point of view[58,134–138]. While the main focus in the early 2010s was primarily the interaction between the axial ligands, nowadays the attention shifted towards the influence the solvation shell and more and more elaborate computational models

are applied[39,55,56,139,140], where the solvent is not only described by an implicit solvation model but rather fully atomistic. To do so, simulations based on, for instance, the empiric valence bond model were used: that model is based on classical molecular mechanics[55,56].

There have been attempts to design computationally better WOCs by modifying their ligand framework. In the following we briefly highlight a few studies where specific properties such as the activation barrier of the O – O bond formation or the coordination strength of ligands have been tuned[135,141–145]. In 2012, Duan *et al.* conducted a DFT-screening approach of axial ligands to overcome the tendency of the axial ligands to dissociate[135]. Correlating the free energy of the ligand-solvent exchange reaction with the highest occupied molecular orbital (HOMO) energy of the ligand allowed them to identify some potential candidates for tightly bound axial ligands which then were synthesized and experimentally tested. Modifications to the bda ligand were later studied by Kang *et al.* where they compared the barriers for the WNA and the I2M mechanisms[142]. They not only replaced the carboxylates with amides but also pyridyls with phenyls and NHCs. The synthetic applicability of the latter might be questionable, however they observed some general trends in terms of barrier heights. In a unique study, the effect of electron withdrawing and donating substituents on the metal coordinated pyridine derivatives was investigated by Asaduzzaman *et al.*[143]. They found that by tuning the electron density at the metal center of a Ru – O_2 species the most stable spin state could be varied. The latter is crucial since the catalysts are expected to evolve triplet oxygen. Stabilization of a triplet state for Ru – O_2 would therefore mean a facile O_2 liberation.

4.2. Modifying the bda Ligand

[Figure 10 about here.]

Using the biqa catalyst, in a chemical water oxidation setup with CAN as a sacrificial oxidant, with either pic or isoq as axial ligands, the reaction was

found to obey a first-order rate-law with respect to the catalyst concentration. This implies that a WNA rather than a I2M mechanism governs the O–O bond formation. Surprisingly, the initial rates (0-4s) of the two catalysts were determined to be vastly different, while the TOFs for the remaining period (4-20s) were almost identical ($0.63s^{-1}$ (pic) and $0.57s^{-1}$ (isoq)). Those values were similar to the ones reported for Ru-bda-pic measured under the same conditions[40]. This is reminiscent of a study on Ru-bda-pic/isoq conducted by Duan *et al*; the initial TOF of the isoq bearing catalyst was significantly higher than the one with pic as axial ligand.

In order to understand this behavior we conducted a DFT study employing standard protocols including implicit solvation by using COSMO. As for the Ru-bda complexes[146], we assumed a sevenfold-coordinated Ru(V)=O species as the key intermediate. The barriers for the WNA mechanism were calculated for both biqa and bda ligands, which showed that the influence of axial ligands on the barrier is minimal. As already observed by others, a carboxylate functioned as an intramolecular base during the reaction mechanism, stabilizing the formed hydroperoxo-species[40]. Likewise we observed that the introduction of an additional water molecule acting as a proton shuttle between the nucleophilic water and the carboxylate lowers the barrier. This finding might be somewhat artificial, since in the absence of solvent - stabilization of a hydronium in close proximity to the positively charged catalysts is energetically unfavorable, especially if the ion is not stabilized by a sufficiently large hydrogen bond network. The barriers for the WNA were then compared with the ones for the I2M mechanism (see Fig. 11). The latter were obtained by performing scans along the constrained O–O bond. Due to the bulkiness of the catalysts there were several conformers possible with various degrees of $\pi - \pi$ stacking. This became more complex by the fact that the two ^{1}[Ru(V)=O] species could obtain an (open shell) singlet or triplet spin state. As a consequence the barriers for the O–O bond formation have to be interpreted with caution. We found that the barriers for the I2M mechanism and WNA are quite similar for both catalysts, and therefore cannot fully explain the different initial rates. Analysis of the post-catalytic

solutions by high performance liquid chromatography (HPLC) revealed for both catalysts free biqa ligand in solution. The latter suggests that the catalysts were unstable under reaction conditions and potentially deactivated after a few turnovers. Those observations also raised the questions regarding what is the 'true' active species, and whether it is the same for both catalysts.

[Figure 11 about here.]

4.3. More Complex Polypyridine Ligands

Another type of ligand modification has recently received a lot of attention, namely the introduction of an additional pyridine subunit into the bda ligand[147], resulting in tda ([2,2′:6′,2″-terpyridine]-6,6″-dicarboxylate) (see Fig. 12). A complete rehearsal of all the studies related to Ru-tda catalysts is beyond the scope of this work and we refer the reader to corresponding publications by Matheu *et al.*[147–149]. Nevertheless, we want to point out some of their characteristic features: First, the first-order kinetics in terms of the catalyst concentration which suggests a WNA mechanism for the O−O bond formation; secondly, flexibility of the tda ligand which can change its coordination mode and therefore adopt to changing ionic radii; thirdly, the decoordination of a carboxylate, which enables the latter to act as an intramolecular base and thereby potentially facilitates a WNA. In two recent studies the role of this carboxylate was investigated by means of AIMD[42] and by means of standard DFT protocols, where the emphasis focused on the pH dependent mechanism[150].

Beside the carboxylate bearing ligands, there is also a huge number of Ru-based catalysts which possess polypyridine ligands or derivatives thereof. Among them is a family discovered by Thummel and coworkers, the mononuclear version of which contains npm (4-t-butyl-2,6-di(1′,8′-naphthyrid-2′-yl)-pyridine) as well as two pic in the axial position (see Fig. 12)[151–157]. The npm ligand contains five basic nitrogen atoms which potentially could coordinate to the metal center, however the geometrical constraint of the naphthyrid-subunit in fact limits the denticity of the npm ligand to three. As a consequence, the metal ion is not completely locked inside the ligand pocket and, as for the bda

catalysts, decoordination of axial ligands might be possible deactivation routes. A possible approach to overcome this is the usage of a higher denticity, such as pentadentate tetrapyridine ligands introduced into the field of Ru-based WOCs by Zhao and cowokers[158,159]. However, those ligands include ethylene linkages which potentially are susceptible to oxidation under catalytic conditions.

[Figure 12 about here.]

4.4. Pentapyridine based Ru-WOCs

In 2017, Gil-Sepulcre *et al.* overcame this shortcoming by the development of the pentadentate ligand Py5R (6,6″-(R(pyridin-2-yl)methylene)-di-2,2′-bipyridine, where R is either a methoxy- or methyl group) (see Fig. 14). The main framework consists of two bipyridines and a pyridine covalently linked at a tertiary carbon[160,161]. On one hand this ligand has the great advantage that the axial pyridine is covalently linked and therefore cannot diffuse away upon decoordination, on the other hand the ligand restricts the accessibility of the Ru-center and therefore potentially prevents the formation of a seven-fold intermediate which was noticed to be advantageous for many other Ru-based catalysts[146]. Surprisingly it was found that the catalytic performance of $[Ru(Py_5OMe)(OH_2)]^{3+}$ obtained by a ligand exchange reaction from $[Ru(Py_5OMe)(Cl)]^{2+}$ was inferior to its precatalyst $[Ru(Py_5OMe)(Cl)]^{2+}$ (TOF: 0.037 vs. 0.710). Those observations, together with a previous study on the *cis* / *trans* isomerization of the ligand[160], led to the conclusion that the pyridyl subunit is indeed able to decoordinate and has to be replaced by an aqua ligand in order to be able to catalyze water oxidation.

What Makes the Difference Between PyOMe and PyMe Catalysts?

Unexpectedly, the catalytic performance of the two catalysts with the very similar ligands Py5OMe and Py5Me turned out to be rather different. At first glance this is difficult to rationalize since the different functional groups are neither directly coordinated to the metal center nor part of a conjugate system and therefore hardly alter the electronics of the metal center. There is also no

significant steric difference, in particular with respect to the suspected WNA mechanism. In order to verify this hypothesis we conducted a full-scale DFT study where we compared the two catalysts in terms of their thermodynamics and kinetics. Investigating the differences in free energy relating to possible intermediates of the catalytic cycle, the thermodynamics of the whole catalytic cycle were comparable among the two catalysts. Differences if there were any, were within the error margin of DFT, except for the substitution of the pyridine with a water molecule - either at the Ru(II) or Ru(III) stage.

The decoordination of the pyridine followed by an association of solvent molecule was found to be thermodynamically more favorable in the case of the Py5OMe WOC. We did not attempt to calculate a transition state for this reaction, due to the unknown nature of the reaction (concerted vs. step-wise, a possible involvement of solvent molecules etc.). Instead, we focused our attention towards the barrier of the WNA forming the O−O bond. The latter is especially interesting for the WOCs at hand, since they possess a decoordinated pyridine in close proximity that is restricted in its conformational freedom due to its covalent linkage to the metal coordinated bipyridyl fragments. The pyridine may thus likely act as proton acceptor which facilitates the WNA by deprotonating the approaching water molecule. This was confirmed by our calculations which revealed a concerted mechanism for the O−O bond formation and the concurrent deprotonation of the nucleophile by the pyridine (see Fig. 13).

[Figure 13 about here.]

The barriers for the two catalysts were, like the thermodynamics, very similar, i.e. 16 kcal/mol (Py5OMe) vs. 14 kcal/mol (Py5Me) in terms of absolute barriers - relative to the Ru(V)=O species and two water molecules at infinite distance. The differences were even smaller when comparing barriers relative to their respective associated reactants, i.e. an encounter complex of Ru(V)=O species and two water molecules. In this case the barrier for both catalysts was found to be of 9 kcal/mol. Those barriers suggest that the O−O bond forma-

tion is not the distinguishing factor for the different catalytic activities of the catalysts featuring Py5OMe and Py5Me.

In an exhaustive kinetic study our experimental co-workers determined several rates of ligand exchange reactions such as the chlorido-water and the pyridine-water exchange (see Fig. 14). While most ligand exchange rates were similar for both ligands, the ones for the chlorido-water exchange were found to favor the Py5Me catalyst by an order of magnitude. The faster chlorido exchange therefore suggests that the Py5Me deactivates more quickly than the Py5OMe species which results in an overall poorer catalytic performance. In a follow-up study we further investigated the role of chlorido-water exchange by calculating transition states for a concerted reaction mechanism[162]. We found that - independent of the oxidation state of the metal center - the (absolute) barriers in the case of the Py5Me catalyst were about 4 kcal/mol smaller than the corresponding ones for Py5OMe bearing WOC. Those differences might be caused by the sterical clash of the substituent at the tertiary carbon with the two bipyridine subunits. The latter is smaller in the case of OMe since the oxygen atom acts as a spacer between the methyl group and the rest of the ligand.

[Figure 14 about here.]

Another potential bottleneck in the catalytic pathway might be the dissociation of the pyridine ligand. Since the nature of this reaction remains unknown, i.e. concerted, step-wise, solvent assisted etc. we decided to conduct dissociation scans of the $N_{Py}-Ru$ bond as well as of the H_2O-Ru bond. The decoordination of the pyridine appears to be favorable in the case of the Py5OMe ligand while the dissociation of the water ligand is less favorable (see Fig. 15). Those scans are in agreement with calculations of the thermodynamics which rendered the displacement of pyridine by water more favorable in the case of Py5OMe.

To summarize the results, the difference in catalytic performance between the two catalysts featuring Py5OMe and Py5Me cannot be rationalized by simply looking at the water oxidation mechanism. As suggested by both experimental results as well as DFT calculations, side reactions, namely the chlorido-water

exchange followed by a pyridine-water substitution, lead to a trans-diaqua complex which presumably is inactive for water oxidation. Further the energetics of the formation of the active catalyst, i.e. the pyridine-water exchange, is also different for the two ligands. A combination of those two factors, the faster rate of a reaction leading to the deactivation of the catalyst as well as a potentially slower rate to form the active catalyst lead to the overall inferior performance of the catalyst featuring Py5Me compared to the one with Py5OMe.

[Figure 15 about here.]

Rational Ligand Design

Since altering the dissociation behavior of a chlorido substituent is not a straightforward process, we were curious whether other modifications of the catalyst could enhance its catalytic performance. So we computationally modified the Py5OMe ligand in order to improve the water oxidation capability by introducing substituents at the dangling pyridine. The electronics of a pyridine and thereby the basicity of the nitrogen atom can easily be changed by placing functional groups in the *ortho*, *meta*, or *para* position. Such modifications are in principle also experimentally feasible, however the practicability has to be tested for each individual case. In a first step we checked whether such substitutions would affect the formation of the active catalyst, i.e. the $N_{Py}-Ru$ bond dissociation. For substituents in either the *meta* or *para* position we noticed a marginal difference, while *ortho* substituents in particular CF_3 led to a larger equilibrium bond distance and therefore weaker bond, as did to a smaller extent OMe. The latter suggests that *ortho* substituents affect both the sterics as well as the electronics of the system. Having established that entering the catalytic cycle should not be affected by the newly introduced substituents, we continued calculating the (absolute) barriers for the $O-O$ bond formation. In general, substituents at the *ortho* position increased the barrier, in particular if the substituents were electron withdrawing and bulky at the same time such as CF_3. The size of substituents introduced in the *para* position has no compelling effect on the barrier, however electron donating substituents have the tendency

to significantly lower the barrier - as illustrated by *p*-OMe, where the barrier went down to 12 kcal/mol compared to 16 kcal/mol for the unmodified pyridine.

Therefore this modification has the potential to enhance drastically the catalytic performance of the catalyst. To further verify this finding, we also compared the thermodynamics i.e. the change in free energy for the initial ET and PCET reactions that are part of the proposed water oxidation mechanism. There the influence was again minimal, which was also expected since the pyridine is not directly affecting the electronics at the metal center. In case the latter is desired, the concept of an thermodynamical 'ideal' catalyst becomes handy. The latter assumes that the water oxidation reaction is free of kinetic barriers, which implies that the minimal electrochemical force required to drive the reaction is equal to one forth of the 4.92 eV necessary for water oxidation (see Eq. 1). The comparison of the 'overall' thermodynamics of a catalyst or of potential WOC candidates obtained from *in silico* design, to a thermodynamically 'ideal' catalyst can serve as a design criterion to identify the promising candidates.

We analyzed various properties such as the spin density of the Ru center and the oxo-ligand, as well as the LUMO-energy of the associated reactant, the transition state and the associated product of the O−O bond formation as possible descriptors for the WNA reaction. Thereby, we found an indirect proportionality between the spin density at the oxo-ligand and barrier height. The latter suggests that a high spin density is consistent with larger electrophilicity of the oxo-ligand.[162].

This study shows that on one hand the system has to be understood very well in order to rationally design and improve an existing system. On the other hand it appears that tuning of certain properties might be more straightforward than others, e.g. whereby one often faces the challenge not to deteriorate one aspect when improving another one.

5. Summary and Conclusion

In the previous sections we gave an brief overview on the computational methodology used to model transition metal based water oxidation catalysts, and how such calculations together with experiments can help to explain their catalytic behavior. We have set the focus on bioinspired Co(II)-cubanes, where we have shown how the speciation of the catalyst in solution opens up alternative reaction pathways. In this context it has been demonstrated how important the choice of an appropriate solvation model is. While explicit solvation, in particular in a dynamic set-up, is often necessary for an accurate description of a species that interacts with solvent, for example through hydrogen bonds, it is also obvious that an atomistic description of the solvent significantly increases the computational cost. For certain properties though, extensions to commonly employed implicit solvation models that account in a better way for such interactions might be a feasible alternative to explicit solvation. Our (dynamic) computational approach with explicit solvation provided not only unprecedented insight into possible water oxidation pathways of Co(II)-based cubanes but also into important properties influencing catalytic activities. The calculations, for instance revealed that a more flexible ligand shell and cubane core, together with a facile change of protonation states and redox-isomerism are factors improving the catalytic effectiveness of $\{Co_3Er(pyMeO)_4\}$ and $\{Co_3Tm(pyMeO)_4\}$ compared to $\{Co_4(pyMeO)_4\}$. Moreover our calculations revealed the possibility that some hydroxido ligands of $\{Co_3Ln(pyMeO)_4\}$ might be involved in the O−O bond formation by acting as an intramolecular base.

In the second part, we used mononuclear Ru-based WOCs to showcase how rational ligand design can lead to more effective catalysts. While most of those design processes are driven by the experimental work, there were also attempts made to invert the order and to computationally predict the effect of certain modifications. However, the latter requires an in-depth understanding of the underlying catalytic mechanism as well as a model system that is able to encompass all important aspects of the system that is to be improved. Knowledge of the lat-

ter is often hard to come by since under experimental conditions often different productive reaction pathways are competing with several deactivation pathways. This makes it difficult to pin-down a single property which might be targeted by the design process. For instance using pentapyridine based Ru-WOCs, we illustrated how this can be achieved using *in silico* design in combination with experimentally available data. In view of the increasing computational power and better modeling approaches this approach will become more important in the future.

6. Acknowledgment

We thank the experimental co-workers in the groups of Alberto, Llobet, and Patzke for the collaboration and fruitful discussion. The work has been supported by the University of Zurich Research Priority Program "Solar Light to Chemical Energy Conversion" (LightChEC) and the Swiss National Science Foundation (grant no. PP00P2_170667).

[1] Huber, M.; Knutti, R. *Nat. Geosci.* **2011**, *5*, 31–36.

[2] Gudmundsson, L.; Seneviratne, S. I.; Zhang, X. *Nat. Clim. Change* **2017**, *7*, 813–816.

[3] Schiermeier, Q. *Nature* **2018**, *560*, 20–22.

[4] United Nations / Framework Convention on Climate Change(2015), - **2015**, –.

[5] Denholm, P.; O'Connell, M.; Brinkman, G.; Jorgenson, J. *National Renewable Energy Laboratory* **2015**, –.

[6] Reece, S. Y.; Hamel, J. A.; Sung, K.; Jarvi, T. D.; Esswein, A. J.; Pijpers, J. J. H.; Nocera, D. G. *Science* **2011**, *334*, 645–648.

[7] Nocera, D. G. *Acc. Chem. Res.* **2012**, *45*, 767–776.

[8] Li, L.; Duan, L.; Xu, Y.; Gorlov, M.; Hagfeldt, A.; Sun, L. *Chem. Commun.* **2010**, *46*, 7307–7309.

[9] Shaffer, D. W.; Xie, Y.; Concepcion, J. J. *Chem. Soc. Rev.* **2017**, *46*, 6170–6193.

[10] Schilling, M.; Luber, S. *Front Chem* **2018**, *6*, 100.

[11] Liu, X.; Wang, F. *Coord. Chem. Rev* **2012**, *256*, 1115–1136.

[12] Singh, A.; Spiccia, L. *Coord. Chem. Rev* **2013**, *257*, 2607–2622.

[13] Najafpour, M. M.; Renger, G.; Hołyńska, M.; Moghaddam, A. N.; Aro, E.-M.; Carpentier, R.; Nishihara, H.; Eaton-Rye, J. J.; Shen, J.-R.; Allakhverdiev, S. I. *Chem. Rev.* **2016**, *116*, 2886–2936.

[14] Tong, L.; Thummel, R. P. *Chem. Sci.* **2016**, *7*, 6591–6603.

[15] Yamamoto, M.; Tanaka, K. *ChemPlusChem* **2016**, *81*, 1028–1044.

[16] Li, J.; Güttinger, R.; Moré, R.; Song, F.; Wan, W.; Patzke, G. R. *Chem. Soc. Rev.* **2017**, *46*, 6124–6147.

[17] Dau, H.; Limberg, C.; Reier, T.; Risch, M.; Roggan, S.; Strasser, P. *ChemCatChem* **2010**, *2*, 724–761.

[18] Sala, X.; Maji, S.; Bofill, R.; García-Antón, J.; Escriche, L.; Llobet, A. *Acc. Chem. Res.* **2014**, *47*, 504–516.

[19] Blakemore, J. D.; Crabtree, R. H.; Brudvig, G. W. *Chem. Rev.* **2015**, *115*, 12974–13005.

[20] Li, Y.-Y.; Ye, K.; Siegbahn, P. E. M.; Liao, R.-Z. *ChemSusChem* **2017**, *10*, 903–911.

[21] Liao, R.-Z.; Siegbahn, P. E. M. *ChemSusChem* **2017**, *10*, 4225–4225.

[22] Vogiatzis, K. D.; Polynski, M. V.; Kirkland, J. K.; Townsend, J.; Hashemi, A.; Liu, C.; Pidko, E. A. *Chem. Rev.* **2019**, *119*, 2453–2523.

[23] Ashley, D. C.; Baik, M.-H. *ACS Catal.* **2016**, *6*, 7202–7216.

[24] Sit, P. H.-L.; Car, R.; Cohen, M. H.; Selloni, A. *Inorg. Chem.* **2011**, *50*, 10259–10267.

[25] Thom, A. J. W.; Sundstrom, E. J.; Head-Gordon, M. *Phys. Chem. Chem. Phys.* **2009**, *11*, 11297–11304.

[26] Aullón, G.; Alvarez, S. *Theor. Chem. Acc.* **2009**, *123*, 67–73.

[27] Vidossich, P.; Lledos, A. *Dalton Trans.* **2014**, *43*, 11145–11151.

[28] Reeves, Y., Kyle G.and Kanai **2014**, *141*, 024305.

[29] Roos, B. O.; Taylor, P. R.; Siegbahn, P. E. *Chem. Phys.* **1980**, *48*, 157–173.

[30] Olsen, J.; Roos, B. O.; Jørgensen, P.; Jensen, H. J. A. **1988**, *89*, 2185–2192.

[31] Malmqvist, P. A.; Rendell, A.; Roos, B. O. *The Journal of Physical Chemistry* **1990**, *94*, 5477–5482.

[32] Fleig, T.; Olsen, J.; Marian, C. M. **2001**, *114*, 4775–4790.

[33] Dongxia, M.; Li Manni, G.; Gagliardi, L. **2011**, *135*, 044128.

[34] Venturinelli Jannuzzi, S. A.; Phung, Q. M.; Domingo, A.; Formiga, A. L. B.; Pierloot, K. *Inorg. Chem.* **2016**, *55*, 5168–5179.

[35] Sparta, M.; Neese, F. *Chem. Soc. Rev.* **2014**, *43*, 5032–5041.

[36] Liakos, D. G.; Sparta, M.; Kesharwani, M. K.; Martin, J. M. L.; Neese, F. *J. Chem. Theory Comput.* **2015**, *11*, 1525–1539.

[37] Saitow, M.; Becker, U.; Riplinger, C.; F., V. E.; Neese, F. **2017**, *146*, 164105.

[38] Hetterscheid, D.; van der Vlugt, J.; de Bruin, B.; Reek, J. *Angw. Chem. Int. Ed.* **2009**, *48*, 8178–8181.

[39] Nyhlén, J.; Duan, L.; Åkermark, B.; Sun, L.; Privalov, T. *Angw. Chem. Int. Ed.* **2010**, *49*, 1773–1777.

[40] Tong, L.; Duan, L.; Xu, Y.; Privalov, T.; Sun, L. *Angw. Chem. Int. Ed.* **2011**, *50*, 445–449.

[41] Scherrer, D.; Schilling, M.; Luber, S.; Fox, T.; Spingler, B.; Alberto, R.; Richmond, C. J. *Dalton Trans.* **2016**, *45*, 19361–19367.

[42] Govindarajan, N.; Tiwari, A.; Ensing, B.; Meijer, E. J. *Inorg. Chem.* **2018**, *57*, 13063–13066.

[43] Evangelisti, F.; Moré, R.; Hodel, F.; Luber, S.; Patzke, G. R. *J. Am. Chem. Soc.* **2015**, *137*, 11076–11084.

[44] Plessow, P. *J. Chem. Theory Comput.* **2013**, *9*, 1305–1310.

[45] Henkelman, G.; Jónsson, H. *J. Chem. Phys.* **2000**, *113*, 9978–9985.

[46] Henkelman, G.; Uberuaga, B. P.; Jónsson, H. *J. Chem. Phys.* **2000**, *113*, 9901–9904.

[47] Laio, A.; Parrinello, M. *Proc Natl Acad Sci USA* **2002**, *99*, 12562–12566.

[48] Barducci, A.; Bonomi, M.; Parrinello, M. *WIREs Comput Mol Sci.* **2011**, *1*, 826–843.

[49] Barducci, A.; Bussi, G.; Parrinello, M. *Phys. Rev. Lett.* **2008**, *100*, 020603.

[50] Dama, J. F.; Rotskoff, G.; Parrinello, M.; Voth, G. A. *J. Chem. Theory Comput.* **2014**, *10*, 3626–3633.

[51] Gil-Ley, A.; Bussi, G. *J. Chem. Theory Comput.* **2015**, *11*, 1077–1085.

[52] Vallés-Pardo, J. L.; Guijt, M. C.; Iannuzzi, M.; Joya, K. S.; de Groot, H. J. M.; Buda, F. *Chem. Phys. Chem.* **2012**, *13*, 140–146.

[53] Piccinin, S.; Sartorel, A.; Aquilanti, G.; Goldoni, A.; Bonchio, M.; Fabris, S. *Proc Natl Acad Sci USA* **2013**, *110*, 4917–4922.

[54] Hodel, F. H.; Deglmann, P.; Luber, S. *J. Chem. Theory Comput.* **2017**, *13*, 3348–3358.

[55] Zhan, S.; Mårtensson, D.; Purg, M.; Kamerlin, S. C. L.; Ahlquist, M. S. G. *Angw. Chem. Int. Ed.* **2017**, *56*, 6962–6965.

[56] Zhan, S.; Zou, R.; Ahlquist, M. S. G. *ACS Catal.* **2018**, *8*, 8642–8648.

[57] Warshel, A. *Computer Modeling of Chemical Reactions in Enzymes and Solutions*, 1st ed.; Wiley Professional; Wiley-Interscience, 1997.

[58] Wang, L.; Duan, L.; Stewart, B.; Pu, M.; Liu, J.; Privalov, T.; Sun, L. *J. Am. Chem. Soc.* **2012**, *134*, 18868–18880.

[59] Klamt, A. *WIREs Comput Mol Sci.* **2011**, *1*, 699–709.

[60] Cramer, C. J.; Truhlar, D. G. *Chem. Rev.* **1999**, *99*, 2161–2200.

[61] Tomasi, J. *Acc. Chem. Res.* **2004**, *112*, 184–203.

[62] Tomasi, J.; Cancés, E.; Pomelli, C. S.; Caricato, M.; Scalmani, G.; Frisch, M. J.; Cammi, R.; Basilevsky, M. V.; Chuev, G. N.; Mennucci, B. *Continuum Solvation Models in Chemical Physics*; John Wiley & Sons, Ltd, 2007.

[63] Skyner, R. E.; McDonagh, J. L.; Groom, C. R.; van Mourik, T.; Mitchell, J. B. O. *Phys. Chem. Chem. Phys.* **2015**, *17*, 6174–6191.

[64] Klamt, A.; Jonas, V.; Bürger, T.; Lohrenz, J. C. W. *J. Phys. Chem. A* **1998**, *102*, 5074–5085.

[65] Ho, J.; Klamt, A.; Coote, M. L. *J. Phys. Chem. A* **2010**, *114*, 13442–13444.

[66] Baik, M.-H.; Friesner, R. A. *J. Phys. Chem. A* **2002**, *106*, 7407–7412.

[67] Hodel, F. H.; Luber, S. *ACS Catal.* **2016**, *6*, 6750–6761.

[68] Ho, J.; Coote, M. L. *Theor. Chem. Acc.* **2009**, *125*, 3.

[69] Marenich, A. V.; Ho, J.; Coote, M. L.; Cramer, C. J.; Truhlar, D. G. *Phys. Chem. Chem. Phys.* **2014**, *16*, 15068–15106.

[70] Zhan, C.-G.; Dixon, D. A. *J. Phys. Chem. A* **2001**, *105*, 11534–11540.

[71] Keith, J. A.; Grice, K. A.; Kubiak, C. P.; Carter, E. A. *J. Am. Chem. Soc.* **2013**, *135*, 15823–15829.

[72] Ho, J. *Phys. Chem. Chem. Phys.* **2015**, *17*, 2859–2868.

[73] Jaque, P.; Marenich, A. V.; Cramer, C. J.; Truhlar, D. G. *J. Phys. Chem. C* **2007**, *111*, 5783–5799.

[74] Rulíšek, L. *J. Phys. Chem. C* **2013**, *117*, 16871–16877.

[75] Bím, D.; Rulíšek, L.; Srnec, M. *J. Phys. Chem. Lett.* **2016**, *7*, 7–13.

[76] Cheng, J.; Liu, X.; VandeVondele, J.; Sulpizi, M.; Sprik, M. *Acc. Chem. Res.* **2014**, *47*, 3522–3529.

[77] Blumberger, J.; Tavernelli, I.; Klein, M. L.; Sprik, M. **2006**, *124*, 064507.

[78] Sulpizi, M.; Sprik, M. *Phys. Chem. Chem. Phys.* **2008**, *10*, 5238–5249.

[79] Adriaanse, C.; Sulpizi, M.; VandeVondele, J.; Sprik, M. *J. Am. Chem. Soc.* **2009**, *131*, 6046–6047.

[80] Cheng, J.; Sulpizi, M.; Sprik, M. **2009**, *131*, 154504.

[81] Sulpizi, M.; Sprik, M. *J. Phys. Condens. Matter* **2010**, *22*, 284116.

[82] Marcus, R. A. *Rev. Mod. Phys.* **1993**, *65*, 599–610.

[83] Hodel, F. H.; Luber, S. *J. Chem. Theory Comput.* **2017**, *13*, 974–981.

[84] Umena, Y.; Kawakami, K.; Shen, J.-R.; Kamiya, N. *Nature* **2011**, *473*, 55–60.

[85] Siegbahn, P. E. M. *Acc. Chem. Res.* **2009**, *42*, 1871–1880.

[86] Pantazis, D. A.; Ames, W.; Cox, N.; Lubitz, W.; Neese, F. *Angw. Chem. Int. Ed. 51*, 9935–9940.

[87] Yano, J.; Yachandra, V. *Chem. Rev.* **2014**, *114*, 4175–4205.

[88] Vinyard, D. J.; Khan, S.; Brudvig, G. W. *Faraday Discuss.* **2015**, *185*, 37–50.

[89] Lohmiller, T.; Krewald, V.; Sedoud, A.; Rutherford, A. W.; Neese, F.; Lubitz, W.; Pantazis, D. A.; Cox, N. *J. Am. Chem. Soc.* **2017**, *139*, 14412–14424.

[90] Suga, M. et al. *Nature* **2017**, *543*, 131–135.

[91] Wang, J.; Askerka, M.; Brudvig, G. W.; Batista, V. S. *ACS Energy Lett.* **2017**, *2*, 2299–2306.

[92] Askerka, M.; Wang, J.; Brudvig, G. W.; Batista, V. S. *Biochemistry* **2014**, *53*, 6860–6862.

[93] Luber, S.; Rivalta, I.; Umena, Y.; Kawakami, K.; Shen, J.-R.; Kamiya, N.; Brudvig, G. W.; Batista, V. S. *Biochemistry* **2011**, *50*, 6308–6311.

[94] Han, Z.; Horak, K. T.; Lee, H. B.; Agapie, T. *J. Am. Chem. Soc.* **2017**, *139*, 9108–9111.

[95] Zhang, C.; Chen, C.; Dong, H.; Shen, J.-R.; Dau, H.; Zhao, J. *Science* **2015**, *348*, 690–693.

[96] Kanady, J. S.; Lin, P.-H.; Carsch, K. M.; Nielsen, R. J.; Takase, M. K.; Goddard, W. A.; Agapie, T. *J. Am. Chem. Soc.* **2014**, *136*, 14373–14376.

[97] Mukherjee, S.; Stull, J. A.; Yano, J.; Stamatatos, T. C.; Pringouri, K.; Stich, T. A.; Abboud, K. A.; Britt, R. D.; Yachandra, V. K.; Christou, G. *Proc Natl Acad Sci USA* **2012**, *109*, 2257–2262.

[98] Kanady, J. S.; Tsui, E. Y.; Day, M. W.; Agapie, T. *Science* **2011**, *333*, 733–736.

[99] McCool, N. S.; Robinson, D. M.; Sheats, J. E.; Dismukes, G. C. *J. Am. Chem. Soc.* **2011**, *133*, 11446–11449.

[100] Evangelisti, F.; Güttinger, R.; Moré, R.; Luber, S.; Patzke, G. R. *J. Am. Chem. Soc.* **2013**, *135*, 18734–18737.

[101] Wang, L.-P.; Van Voorhis, T. *J. Phys. Chem. Lett.* **2011**, *2*, 2200–2204.

[102] Kwapien, K.; Piccinin, S.; Fabris, S. *J. Phys. Chem. Lett.* **2013**, *4*, 4223–4230.

[103] Li, X.; Siegbahn, P. E. M. *J. Am. Chem. Soc.* **2013**, *135*, 13804–13813.

[104] Fernando, A.; Aikens, C. M. *J. Phys. Chem. C* **2015**, *119*, 11072–11085.

[105] Smith, P. F.; Hunt, L.; Laursen, A. B.; Sagar, V.; Kaushik, S.; Calvinho, K. U. D.; Marotta, G.; Mosconi, E.; De Angelis, F.; Dismukes, G. C. *J. Am. Chem. Soc.* **2015**, *137*, 15460–15468.

[106] Nguyen, A. I.; Ziegler, M. S.; Oa-Burgos, P.; Sturzbecher-Hohne, M.; Kim, W.; Bellone, D. E.; Tilley, T. D. *J. Am. Chem. Soc.* **2015**, *137*, 12865–12872.

[107] Nguyen, A. I.; Wang, J.; Levine, D. S.; Ziegler, M. S.; Tilley, T. D. *Chem. Sci.* **2017**, *8*, 4274–4284.

[108] Zhang, B.; Sun, L. *Dalton Trans.* **2018**, *47*, 14381–14387.

[109] Brodsky, C. N.; Hadt, R. G.; Hayes, D.; Reinhart, B. J.; Li, N.; Chen, L. X.; Nocera, D. G. *Proc Natl Acad Sci USA* **2017**, *114*, 3855–3860.

[110] Wang, T.; Brudvig, G. W.; Batista, V. S. *J. Chem. Theory Comput.* **2010**, *6*, 2395–2401.

[111] Ullman, A. M.; Liu, Y.; Huynh, M.; Bediako, D. K.; Wang, H.; Anderson, B. L.; Powers, D. C.; Breen, J. J.; Abrua, H. D.; Nocera, D. G. *J. Am. Chem. Soc.* **2014**, *136*, 17681–17688.

[112] Genoni, A.; La Ganga, G.; Volpe, A.; Puntoriero, F.; Di Valentin, M.; Bonchio, M.; Natali, M.; Sartorel, A. *Faraday Discuss.* **2015**, *185*, 121–141.

[113] Piccinin, S.; Fabris, S. *Phys. Chem. Chem. Phys.* **2011**, *13*, 7666–7674.

[114] Hodel, F. H.; Luber, S. *ACS Catal.* **2016**, *6*, 1505–1517.

[115] Becke, A. D. *Phys. Rev. A* **1988**, *38*, 3098–3100.

[116] Perdew, J. P. *Phys. Rev. B* **1986**, *33*, 8822–8824.

[117] Becke, A. D. *J. Chem. Phys.* **1993**, *98*, 5648.

[118] Lee, C.; Yang, W.; Parr, R. G. *Phys. Rev. B* **1988**, *37*, 785–789.

[119] Group, C. D. CP2K. `https://www.cp2k.org/`.

[120] Ahlrichs, R.; Bär, M.; Häser, M.; Horn, H.; Kölmel, C. *Chem. Phys. Lett.* **1989**, *162*, 165–169.

[121] Klamt, A.; Schüürmann, G. *J. Chem. Soc., Perkin Trans. 2* **1993**, 799–805.

[122] Schilling, M.; Hodel, F.; Luber, S. *ChemSusChem* **2017**, *10*, 4561–4569.

[123] Cox, N.; Retegan, M.; Neese, F.; Pantazis, D. A.; Boussac, A.; Lubitz, W. *Science* **2014**, *345*, 804–808.

[124] Song, F.; Moré, R.; Schilling, M.; Smolentsev, G.; Azzaroli, N.; Fox, T.; Luber, S.; Patzke, G. R. *J. Am. Chem. Soc.* **2017**, *139*, 14198–14208.

[125] Gersten, S. W.; Samuels, G. J.; Meyer, T. J. *J. Am. Chem. Soc.* **1982**, *104*, 4029–4030.

[126] Gilbert, J. A.; Eggleston, D. S.; Murphy, W. R.; Geselowitz, D. A.; Gersten, S. W.; Hodgson, D. J.; Meyer, T. J. *J. Am. Chem. Soc.* **1985**, *107*, 3855–3864.

[127] Sala, X.; Romero, I.; Rodríguez, M.; Escriche, L.; Llobet, A. *Angw. Chem. Int. Ed.* **2009**, *48*, 2842–2852.

[128] Romain, S.; Vigara, L.; Llobet, A. *Acc. Chem. Res.* **2009**, *42*, 1944–1953.

[129] Cao, R.; Lai, W.; Du, P. *Energy Environ. Sci.* **2012**, *5*, 8134–8157.

[130] Kärkäs, M. D.; Verho, O.; Johnston, E. V.; Åkermark, B. *Chem. Rev.* **2014**, *114*, 11863–12001.

[131] Zeng, Q.; Lewis, F. W.; Harwood, L. M.; Hartl, F. *Coord. Chem. Rev* **2015**, *304-305*, 88 – 101.

[132] Kärkäs, M. D.; Åkermark, B. **2016**, *16*, 940–963.

[133] Duan, L.; Bozoglian, F.; Mandal, S.; Stewart, B.; Privalov, T.; Llobet, A.; Sun, L. *Nat. Chem.* **2012**, *4*, 418–423.

[134] Duan, L.; Xu, Y.; Zhang, P.; Wang, M.; Sun, L. *Inorg. Chem.* **2010**, *49*, 209–215.

[135] Duan, L.; Araujo, C. M.; Ahlquist, M. S.; Sun, L. *Proc Natl Acad Sci USA* **2012**,

[136] Duan, L.; Wang, L.; Inge, A. K.; Fischer, A.; Zou, X.; Sun, L. *Inorg. Chem.* **2013**, *52*, 7844–7852.

[137] Wang, L.; Duan, L.; Wang, Y.; Ahlquist, M. S. G.; Sun, L. *Chem. Commun.* **2014**, *50*, 12947–12950.

[138] Staehle, R.; Tong, L.; Wang, L.; Duan, L.; Fischer, A.; Ahlquist, M. S. G.; Sun, L.; Rau, S. *Inorg. Chem.* **2014**, *53*, 1307–1319.

[139] Fan, T.; Duan, L.; Huang, P.; Chen, H.; Daniel, Q.; Ahlquist, M. S. G.; Sun, L. *ACS Catal.* **2017**, *7*, 2956–2966.

[140] Xie, Y.; Shaffer, D. W.; Concepcion, J. J. *Inorg. Chem.* **2018**, *57*, 10533–10542.

[141] Zhang, G.; Chen, K.; Chen, H.; Yao, J.; Shaik, S. *Inorg. Chem.* **2013**, *52*, 5088–5096.

[142] Kang, R.; Chen, K.; Yao, J.; Shaik, S.; Chen, H. *Inorg. Chem.* **2014**, *53*, 7130–7136.

[143] Asaduzzaman, A. M.; Wasylenko, D.; Berlinguette, C. P.; Schreckenbach, G. *J. Phys. Chem. C* **2015**, *119*, 242–250.

[144] Okamura, M.; Masaoka, S. *Chem. Asian J.* **2015**, *10*, 306–315.

[145] Hessels, J.; Detz, R. J.; Koper, M. T. M.; Reek, J. N. H. *Chem. Eur. J.* **2017**, *23*, 16413–16418.

[146] Duan, L.; Fischer, A.; Xu, Y.; Sun, L. *J. Am. Chem. Soc.* **2009**, *131*, 10397–10399, PMID: 19601625.

[147] Matheu, R.; Ertem, M. Z.; Benet-Buchholz, J.; Coronado, E.; Batista, V. S.; Sala, X.; Llobet, A. *J. Am. Chem. Soc.* **2015**, *137*, 10786–10795.

[148] Matheu, R.; Ertem, M. Z.; Gimbert-Suriñach, C.; Benet-Buchholz, J.; Sala, X.; Llobet, A. *ACS Catal.* **2017**, *7*, 6525–6532.

[149] Matheu, R.; Ertem, M. Z.; Pipelier, M.; Lebreton, J.; Dubreuil, D.; Benet-Buchholz, J.; Sala, X.; Tessier, A.; Llobet, A. *ACS Catal.* **2018**, *8*, 2039–2048.

[150] Wang, Y.; Zhan, S.; Ahlquist, M. S. G. *Organometallics* **2018**, -, –.

[151] Zong, R.; Thummel, R. P. *J. Am. Chem. Soc.* **2005**, *127*, 12802–12803.

[152] Tseng, H.-W.; Zong, R.; Muckerman, J. T.; Thummel, R. *Inorg. Chem.* **2008**, *47*, 11763–11773.

[153] Polyansky, D. E.; Muckerman, J. T.; Rochford, J.; Zong, R.; Thummel, R. P.; Fujita, E. *J. Am. Chem. Soc.* **2011**, *133*, 14649–14665.

[154] Badiei, Y. M.; Polyansky, D. E.; Muckerman, J. T.; Szalda, D. J.; Haberdar, R.; Zong, R.; Thummel, R. P.; Fujita, E. *Inorg. Chem.* **2013**, *52*, 8845–8850.

[155] Muckerman, J. T.; Kowalczyk, M.; Badiei, Y. M.; Polyansky, D. E.; Concepcion, J. J.; Zong, R.; Thummel, R. P.; Fujita, E. *Inorg. Chem.* **2014**, *53*, 6904–6913.

[156] Tong, L.; Zong, R.; Zhou, R.; Kaveevivitchai, N.; Zhang, G.; Thummel, R. P. *Faraday Discuss.* **2015**, *185*, 87–104.

[157] Moonshiram, D.; Pineda-Galvan, Y.; Erdman, D.; Palenik, M.; Zong, R.; Thummel, R.; Pushkar, Y. *J. Am. Chem. Soc.* **2016**, *138*, 15605–15616.

[158] Radaram, B.; Ivie, J. A.; Singh, W. M.; Grudzien, R. M.; Reibenspies, J. H.; Webster, C. E.; Zhao, X. *Inorg. Chem.* **2011**, *50*, 10564–10571.

[159] Vennampalli, M.; Liang, G.; Webster, C. E.; Zhao, X. *Eur. J. Inorg. Chem.* *2014*, 715–721.

[160] Gil-Sepulcre, M.; Axelson, J. C.; Aguiló, J.; Solà-Hernández, L.; Francàs, L.; Poater, A.; Blancafort, L.; Benet-Buchholz, J.; Guirado, G.; Escriche, L.; Llobet, A.; Bofill, R.; Sala, X. *Inorg. Chem.* **2016**, *55*, 11216–11229.

[161] Gil-Sepulcre, M.; Böhler, M.; Schilling, M.; Bozoglian, F.; Bachmann, C.; Scherrer, D.; Fox, T.; Spingler, B.; Gimbert-Suriñach, C.; Alberto, R.; Bofill, R.; Sala, X.; Luber, S.; Richmond, C. J.; Llobet, A. *ChemSusChem* *10*, 4517–4525.

[162] Schilling, M.; Böhler, M.; Luber, S. *Dalton Trans.* **2018**, *47*, 10480–10490.

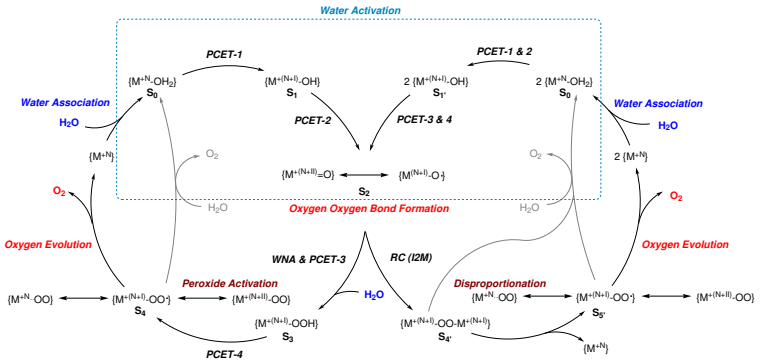

Figure 1: Schematic overview of a possible water oxidation mechanism. M represents any redox active transition metal, N as a superscript represents the formal oxidation state of the metal center in the catalytic resting state. Reactions connecting two states do not necessarily have to be PCETs, various sequences of ET and PT reactions are possible. Further, some catalysts might require an activation step to reach the catalytic ground state.

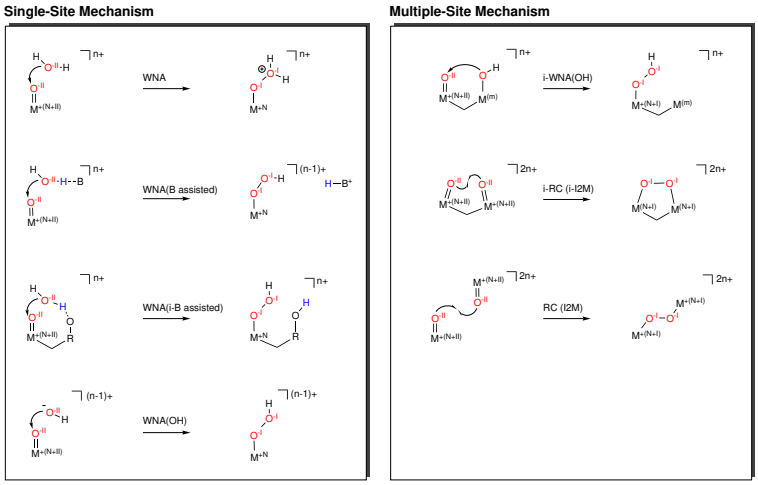

Figure 2: O−O bond formation mechanisms, where M represents any redox-active metal center in the formal oxidation state indicated by the superscript, where +N is used for the 'active' metal center and +m for any spectator metal center. Further the overall charge of the species is denoted as n+, respectively 2n+ in case of a bimolecular reaction. The formal oxidation state N and the overall charge n represent always the same numerical value. The overall charge of the association complex as well as of the product are given to highlight charge conservation. For the sake of clarity the formal oxidation state of the involved oxygen atoms is given in both the reactant and product state. B is a general base in solution, and R is any residue including other transition metals. Reproduced from Schilling and Luber [10].

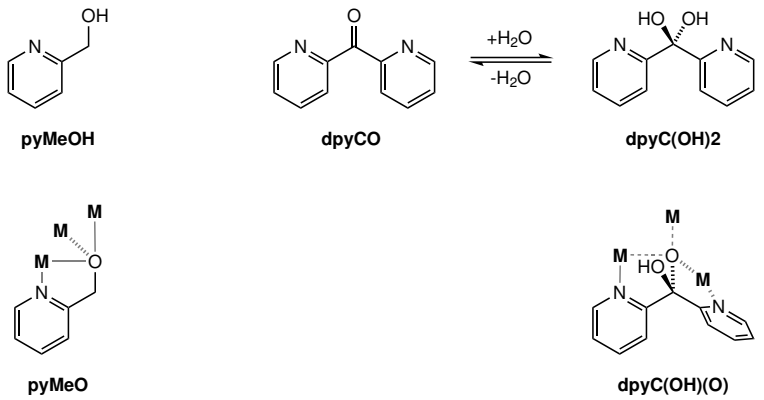

Figure 3: Chemical structure of the pyMeO (pyridin-2-ylmethanolato) and dpyC(OH)(O) (hydroxyldi-2-pyridinylmethanolato) ligand, in their native form (top) and coordinated to several metal centers as in the Co(II)-cubanes. Note how the hydroxide becomes part of the cubane core by coordinating three different metal centers[43,100,124].

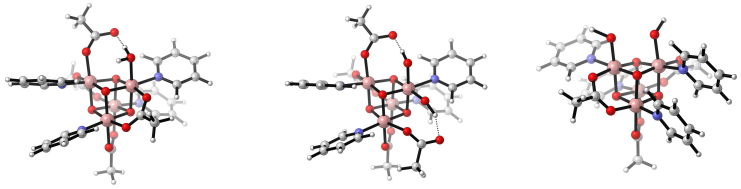

Figure 4: Schematic illustration of $[Co^{III}{}_4(\mu^3\text{-O})_4(\mu^2\text{-OAc})_4(Py)_4]$ where a single water molecule is associated (left,[103]), or either two hydroxido ligands in a geminal- (middle,[105]) or *cis*-configuration (right,[107]). The following color code applies for all illustrations: *white* - hydrogen, *grey* - carbon, *dark blue* - nitrogen, *red* - oxygen, *green* - chlorine, *light pink* - cobalt, *lime* – erbium, thulium, ytterbium or holmium, *dark green* - ruthenium. Reproduced from Schilling and Luber[10].

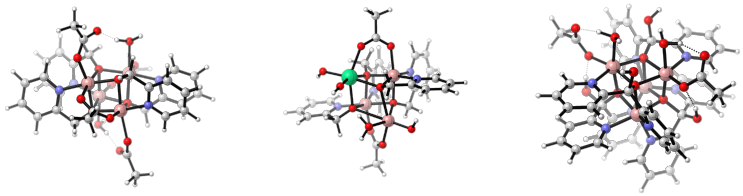

Figure 5: Schematic illustration of the cubanes studied by Patzke and co-workers: $\{Co_4(pyMeO)_4\}$ (left,[100]) and $\{Co_3Ln(pyMeO)_4\}$ (middle,[43]) (Ln = Er, Tm, Yb, Ho. Note: the structure shown is the model system used in Ref.[67] and not the crystal structure shown in Ref.[43]), and the recently published third generation $\{Co_4(dpyC(OH)(O))_4\}$ (right,[124]). Reproduced from Schilling and Luber[10].

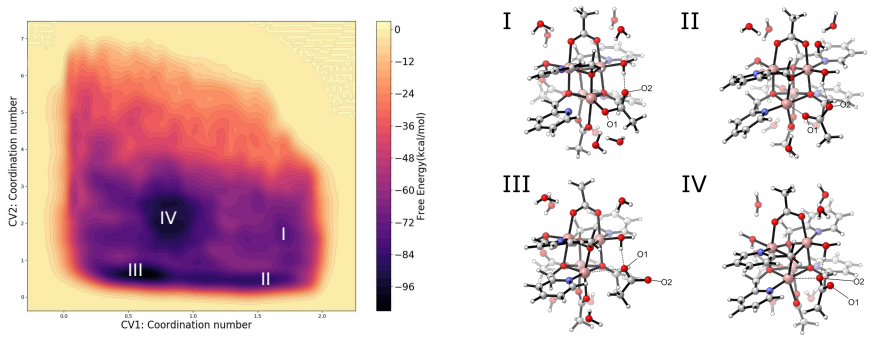

Figure 6: Potential free energy surface of acetate dissociation of $\{Co_4(pyMeO)_4\}$. Several local minima are labeled and a representative structure for each of them is shown. Reproduced from data published by Hodel and Luber [54].

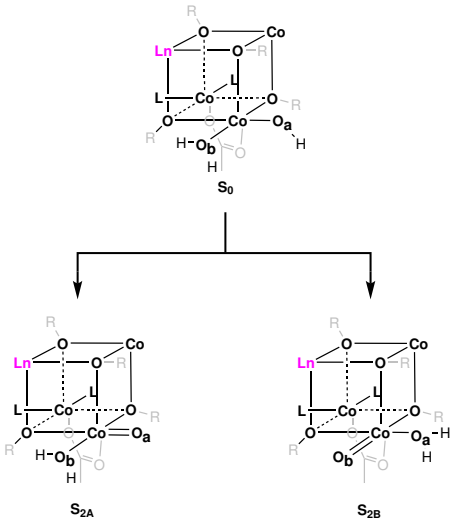

Figure 7: Schematic illustration of selected states of the two possible pathways A (left) and B (right); For the sake of clarity all ligands on the other cobalt or lanthanide cations are not shown, except for the one where the water oxidation takes place,

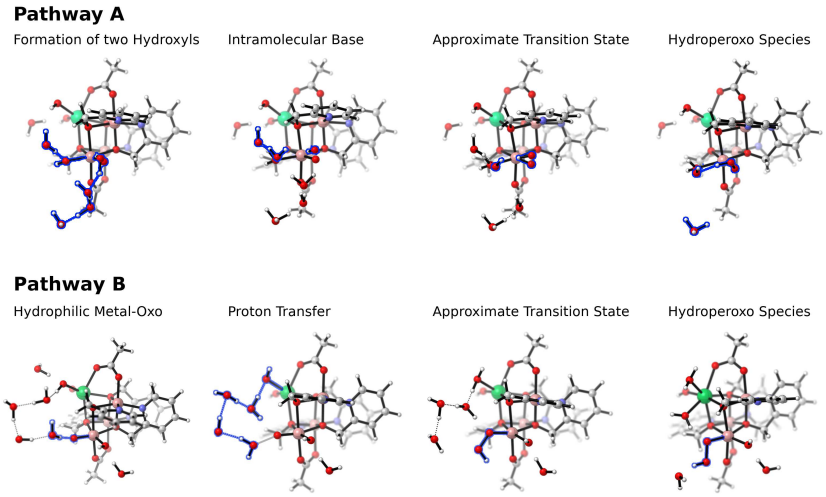

Figure 8: Selected intermediates of the minimum energy pathways for the O−O bond formation of the two possible pathways (A and B) of $[Co^{II}{}_3Er(pyMeO)_4(\mu^2\text{-}2\,OAc)_2(OH)_3H_2O]$. Pathway A (top): Notice the hydronium ion formed in the last structure. Pathway B (bottom): An erbium coordinated hydroxido ligand acts as an intramolecular base that facilitates the formation of the O−O bond.[67]. Reproduced from Schilling and Luber[10].

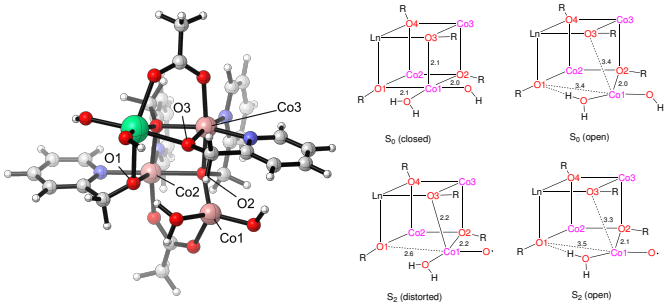

Figure 9: Ball-stick representation of the 'open' form of $\{Co_3Ln(pyMeO)_4\}$ (left). Schematic drawing of the 'closed' and 'open' form discussed in this section, as well as the 'distorted' form already mentioned in the context of the mechanism in the previous section[67]. Reproduced from Ref.[122] - published by John Wiley and Sons.

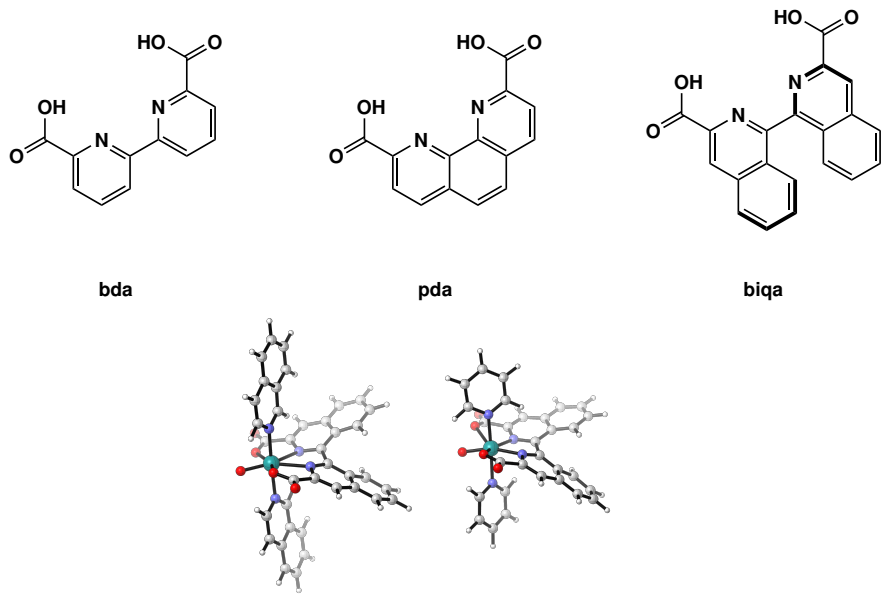

Figure 10: Schematic representation of pyridine based bidicarboxylic acid ligands used for WOC of the type $[Ru(L(R)_2]$, where L = bda, pda or biqa and R = pic or isoq (top). Ball-stick representation of $[Ru(biqa)(isoq)_2]$ and $[Ru(biqa)(pic)_2]$ catalysts investigated by Scherrer *et al.*[41])(bottom). Reproduced from geometrical data published by Scherrer *et al.*[41] (left).

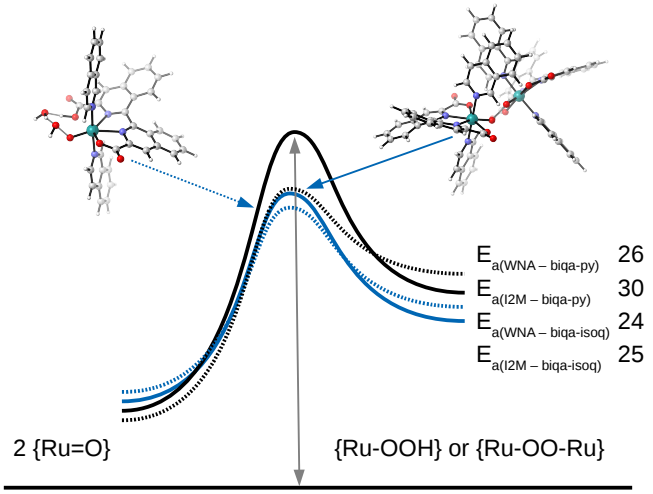

Figure 11: Electronic activation energies for the WNA and I2M mechanism of $[Ru(biqa)(R)_2]$, where R = py (dashed lines) or isoq (solid line). Two exemplary transition state structures are shown, the color and line style are the same as the energy profile. The activation energies are ordered by the stability of the respective product. Note in the case of the WNA mechanism, there is an additional water molecule which acts as a proton shuttle. All energies are given in kcal/mol. Reproduced from data published by Scherrer *et al.*[41].

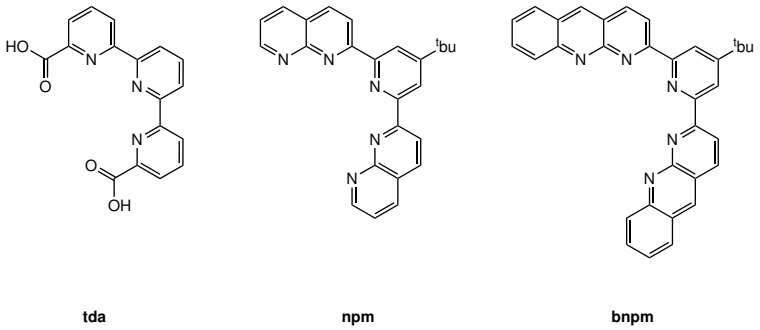

Figure 12: Chemical structures of some selected pyridine based ligands, commonly used in WOC catalysts: tda ([2,2′:6′,2″-terpyridine]-6,6″-dicarboxylate) (left) [147], npm (4-*t*-butyl-2,6-di(1′,8′-naphthyrid-2′-yl)-pyridine) (middle) [151], bnpm (2,6-bis(benzo[*b*]-1′,8′-naphthydridin-2′yl)4-*t*-butylpyridine) (right) [154].

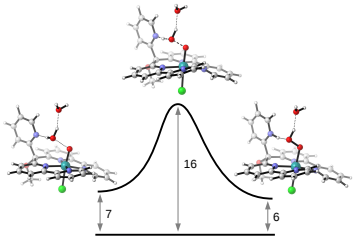

Figure 13: Reaction scheme of the O−O bond formation for a base assisted WNA of $[Ru(Py_5OMe)(Cl)]^{2+}$. All energies are given in kcal/mol. Reproduced from Ref.[162] with permission from The Royal Society of Chemistry.

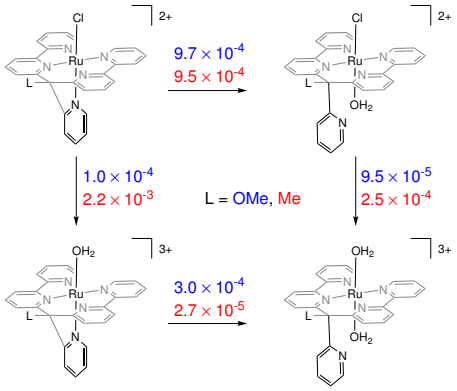

Figure 14: Rate constants for ligand dissociation / association reaction, either experimentally measured or obtained from kinetic modeling of the Py5OMe (blue) and Py5Me (red) bearing catalysts. All rate constants are given in s^{-1}. Adopted from Ref. [161].

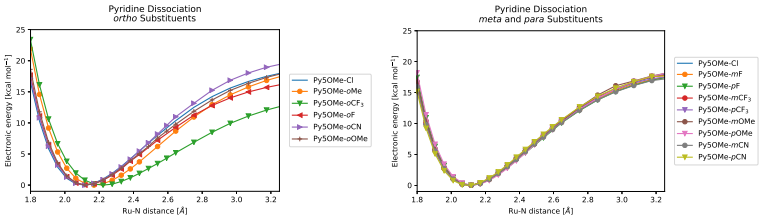

Figure 15: Energy profile of pyridine dissociation reaction - for different substitution patterns at the pyridine of [Ru(Py$_5$OMe)]. Reproduced from Ref.[162] with permission from The Royal Society of Chemistry.